Interval Methods for Robust Sliding Mode Control Synthesis of High-Temperature Fuel Cells with State and Input Constraints

Andreas Rauh and Luise Senkel

Abstract Fuel cell systems provide a way to produce electric energy in future decentralized power supply grids. In the case of using high-temperature fuel cells, it becomes possible to exploit not only the provided electric power but also the process heat in order to maximize the overall system efficiency. However, the efficiency maximization goes along with a high flexibility with respect to temporal variations of the electric power that is demanded by corresponding consumers. Such power variations impose restrictions on intelligent fuel cell control systems. Such control strategies do not only have to make sure that the supplied fuel gas (typically hydrogen and mixtures with methane or carbon monoxide) is stoichiometrically balanced with the demanded electric power. It is also inevitable to control the fuel cell itself from a thermodynamic point of view. This control has to make sure that sufficiently smooth temperature trajectories can be tracked during the heating phase of the system and that a priori unknown but bounded disturbances are robustly compensated at high-temperature operating points. For this purpose, interval-based sliding mode control procedures can be implemented. This contribution gives an overview of how interval methods can be combined with the fundamental sliding mode methodology in a variable-structure control synthesis. The efficiency of the presented methods is highlighted for the control of solid oxide fuel cells in various simulations.

1 Introduction

The control of nonlinear dynamic systems is an important topic for many practical applications. Especially, in cases in which dynamic system models are significantly influenced by uncertain parameters and bounded (additive) uncertainty, it is challenging to determine feedback control procedures that reliably stabilize the

A. Rauh (✉) · L. Senkel
Chair of Mechatronics, University of Rostock,
Justus-von-Liebig-Weg 6, 18059 Rostock, Germany
e-mail: andreas.rauh@uni-rostock.de

L. Senkel
e-mail: luise.senkel@uni-rostock.de

A. Rauh and L. Senkel (eds.), *Variable-Structure Approaches*,
Mathematical Engineering, DOI 10.1007/978-3-319-31539-3_3

system dynamics and—at the same time—guarantee that specific state constraints are not violated. As mentioned in the abstract of this contribution, the control of high-temperature solid oxide fuel cell systems (SOFC systems) belongs to this class of applications.

As shown in previous work, it is possible to use interval arithmetic techniques for the implementation of feedback controllers that can be applied in real time [19–27, 29]. On the one hand, these controllers have to fulfill the requirement of robustness against bounded uncertainty and disturbances. On the other hand, the asymptotic stability of the dynamics of the overall closed-loop control structure has to be shown in a guaranteed way. The basic idea of the chosen control structure is motivated by the principle of sliding mode control [31, 32, 36, 37].

In classical sliding mode techniques, so-called equivalent control strategies are determined for the exact tracking of sufficiently smooth reference trajectories. These equivalent controllers represent the control for states located exactly on the sliding surface, which serves as a specification of the desired closed-loop system dynamics. State values which are not (exactly) located on this sliding surface are forced to converge toward it using a variable-structure control approach. The amplitude of this variable-structure control component is usually selected as a constant in such a way that the influence of uncertain parameters is overcompensated. However, the choice of such constant variable-structure gains may have the drawback of unnecessarily large chattering phenomena. Such chattering should be reduced as far as possible for practical applications to avoid the associated non-advantageous actuator wear and energy consumption [19].

In contrast to classical sliding mode approaches, the fundamental idea of interval-based sliding mode control is the online adaptation of the variable-structure control component with respect to both the current uncertain system state and uncertain parameters, cf. [19, 23, 29]. This computation can be performed in real time using software libraries for basic interval functionalities. For this purpose, the calculation of the control signal is implemented in such a way that asymptotic stability of the closed-loop control system can be shown using suitable candidates for Lyapunov functions. Such candidates were so far investigated for first-order sliding mode control without and with one-sided barrier functions. These barriers serve as a guaranteed means to avoid the violation of hard upper bounds for selected state variables. For example, such upper bounds may represent the maximum admissible temperature of SOFC stacks. One of the important generalizations presented in this contribution is the extension of these techniques to an interval-based sliding mode control of second order as well as a generalization to two-sided barriers.

Section 2 gives an overview of fundamental first- and second-order sliding mode control approaches, their generalization to interval-based implementations, and illustrating simulation examples that highlight the properties and advantages of the chosen options. Thereafter, Sect. 3 describes a brief summary of the control-oriented modeling of the thermal behavior of SOFCs. The control design for these systems is described in Sect. 4 by the presented interval-based variable-structure methods. Representative simulation results are summarized in Sect. 5. Finally, conclusions and an outlook on future work are given in Sect. 6.

2 Sliding Mode Control with Guaranteed State Constraints

In this section, a summary is given for fundamental sliding mode control approaches that can be generalized in two different ways. First, they are generalized in such a way that violations of hard constraints on state variables and deviations of the states from the sliding surface are penalized in a reliable way. This penalization makes use of strict inequalities that are represented using a barrier Lyapunov function approach [9, 17, 35]. Second, techniques are introduced that allow for a verified treatment of uncertainty in the state equations by means of interval arithmetic [11, 14, 16]. These techniques aim at the online computation of control laws in such a manner that chattering due to unnecessarily large switching amplitudes is reduced as much as possible. The usage of these approaches is described for an illustrative example that is similar to the dynamics of the considered fuel cell system after a suitable coordinate transformation.

2.1 Fundamental Sliding Mode Control Laws

Both the treatment of strict inequality constraints and bounded interval uncertainty can be combined with first- and second-order sliding mode techniques. The fundamental stages are the definition of appropriate sliding surfaces and the guaranteed proof of asymptotic stability using suitable candidates for Lyapunov functions.

2.1.1 First-Order Sliding Mode Control

As an illustrative example, the nth-order linear system model

$$\begin{bmatrix} \dot{x}_1(t) \\ \dot{x}_2(t) \\ \vdots \\ \dot{x}_{n-1}(t) \\ \dot{x}_n(t) \end{bmatrix} = \begin{bmatrix} x_2(t) \\ x_3(t) \\ \vdots \\ x_n(t) \\ u(t) \end{bmatrix} \tag{1}$$

with the state vector $\mathbf{x}(t) \in \mathbb{R}^n$ and the scalar control input $u(t) \in \mathbb{R}$ is considered. The system output is represented by the first state variable according to

$$y(t) = x_1(t). \tag{2}$$

Obviously, the dynamic system (1) with the output variable (2) has the relative degree n [12, 15]. This is confirmed by the fact that the nth time derivative $x_1^{(n)}(t) = u(t)$ of the system output is the lowest-order derivative that explicitly depends on the control input $u(t)$. Therefore, the output $y(t)$ corresponds to a (trivial) flat system

output [5] with which the complete system dynamics and suitable feedforward and feedback control approaches can be parameterized for sufficiently smooth desired trajectories $x_{1,\mathrm{d}}(t)$.

Using this desired output, the corresponding tracking error ($r = 0$) and its rth time derivative are given by

$$\tilde{\xi}_1^{(r)}(t) = x_1^{(r)}(t) - x_{1,\mathrm{d}}^{(r)}(t) \tag{3}$$

with $r \in \{0, 1, \ldots, n\}$.

Using the definition (3) of the tracking error, the sliding surface

$$s := s(t) = \sum_{r=0}^{n-1} \alpha_r \tilde{\xi}_1^{(r)}(t) \tag{4}$$

with the normalized coefficient $\alpha_{n-1} = 1$ can be defined. To guarantee asymptotic stability of the system dynamics on this sliding surface, the parameters α_r have to fulfill the necessary and sufficient stability conditions for a Hurwitz polynomial [6] of linear dynamic systems of the order $n - 1$.

First-order sliding mode control approaches can be derived with the help of the quadratic radially unbounded candidate for a Lyapunov function

$$V^{\langle \mathrm{I} \rangle} = \frac{1}{2} s^2 > 0 \quad \text{for} \quad s \neq 0. \tag{5}$$

(Global) Asymptotic stability of the dynamic system corresponds to the (global) negative definiteness of the corresponding time derivative

$$\dot{V}^{\langle \mathrm{I} \rangle} = s \cdot \dot{s} = \left(\sum_{r=0}^{n-1} \alpha_r \tilde{\xi}_1^{(r)}(t) \right) \cdot \left(\sum_{r=0}^{n-1} \alpha_r \tilde{\xi}_1^{(r+1)}(t) \right) < 0 \quad \text{for} \quad s \neq 0. \tag{6}$$

During the derivation of the variable-structure sliding mode control approach [21, 27], the right-hand side of the inequality (6) is replaced by the more conservative formulation

$$\left(\sum_{r=0}^{n-1} \alpha_r \tilde{\xi}_1^{(r)}(t) \right) \cdot \left(\sum_{r=0}^{n-1} \alpha_r \tilde{\xi}_1^{(r+1)}(t) \right) < -\eta \cdot |s| = -\eta \cdot \left(\sum_{r=0}^{n-1} \alpha_r \tilde{\xi}_1^{(r)}(t) \right) \cdot \operatorname{sign}(s) \tag{7}$$

which guarantees global asymptotic stability for arbitrary parameters $\eta > 0$. Note that the actual choice of η significantly influences the dynamics and the maximum absolute values of the control signal in the so-called reaching phase in which $s \neq 0$ holds. As soon as the sliding surface $s = 0$ has been reached in a finite time, the control amplitudes depend on the actual choice of the reference trajectory $x_{1,\mathrm{d}}(t)$ and on the coefficients α_r. The latter values have the major influence on the control

amplitudes as soon as non-modeled errors and disturbances influence the system dynamics and if the error signals $\tilde{\xi}_1^{(r)}(t)$ are corrupted by non-negligible measurement noise or state reconstruction errors.

The derivation of the control law is completed by enforcing that the second factor in (7) becomes proportional to the sign of the actual value of s according to

$$\left(\sum_{r=0}^{n-1} \alpha_r \tilde{\xi}_1^{(r)}(t)\right) \cdot \underbrace{\left(\sum_{r=0}^{n-2} \alpha_r \tilde{\xi}_1^{(r+1)}(t) + u(t) - x_{1,\mathrm{d}}^{(n)}(t) + \eta \cdot \operatorname{sign}(s)\right)}_{-\beta \cdot \operatorname{sign}(s)} < 0 \tag{8}$$

with $\beta > 0$. The definition of $\tilde{\eta} := \eta + \beta > 0$ leads to the final control signal

$$u(t) = u^{\langle \mathrm{I} \rangle}(t) = x_{1,\mathrm{d}}^{(n)}(t) - \sum_{r=0}^{n-2} \alpha_r \tilde{\xi}_1^{(r+1)}(t) - \tilde{\eta} \cdot \operatorname{sign}(s)\,. \tag{9}$$

In principle, the robustness of the closed-loop control system can be improved by adding the integral of the tracking error with a suitable gain value to the definition of the sliding surface. Such additional measures are investigated in the following subsection for the derivation of second-order sliding mode controllers.

2.1.2 Second-Order Sliding Mode Control

A second-order sliding mode is defined in the sense that not only $s = s(t) = 0$ but also $\dot{s} = \dot{s}(t) = 0$ are ensured by the designed feedback controller [1, 4, 7]. This can be achieved by additionally low-pass filtering (first-order lag dynamics) the left-hand side of

$$\gamma_1 \dot{s} + \gamma_0 s = \sum_{r=0}^{n-1} \alpha_r \tilde{\xi}_1^{(r)}(t). \tag{10}$$

For the sake of asymptotic stability, the coefficients γ_0 and γ_1 need to be strictly positive, while the coefficients on the right-hand side of (10) are again chosen as parameters of a Hurwitz polynomial of the order $n - 1$. As before, this sliding surface has a PD (proportional, differentiating) characteristic.

To enhance steady-state accuracy, the sliding surface in (10) is extended by an additional time integral of the tracking error with

$$\gamma_1 \dot{s} + \gamma_0 s = \alpha_{-1} \int_0^t \tilde{\xi}_1(\tau)\mathrm{d}\tau + \sum_{r=0}^{n-1} \alpha_r \tilde{\xi}_1^{(r)}(t). \tag{11}$$

For a short-hand notation, this extension of the sliding surface (11) is abbreviated by

$$\gamma_1 \dot{s} + \gamma_0 s = \sum_{r=-1}^{n-1} \alpha_r \tilde{\xi}_1^{(r)}(t) \quad \text{with} \quad \tilde{\xi}_1^{(-1)}(t) := \int_0^t \tilde{\xi}_1(\tau) \mathrm{d}\tau. \tag{12}$$

The second time derivative of the PID-type sliding variable s, required subsequently for the control design, is given by the differentiation of (11), (12) and subsequently solving it for $\ddot{s}$ with

$$\ddot{s} = -\frac{\gamma_0}{\gamma_1}\dot{s} + \frac{1}{\gamma_1} \sum_{r=-1}^{n-1} \alpha_r \tilde{\xi}_1^{(r+1)}(t) = -\frac{\gamma_0}{\gamma_1}\dot{s} + \frac{1}{\gamma_1} \sum_{r=0}^{n} \alpha_{r-1} \tilde{\xi}_1^{(r)}(t). \tag{13}$$

Here, the special case $\alpha_{-1} \equiv 0$ corresponds to the case of a sliding surface of PD type. In analogy to the previous subsection, an appropriate Lyapunov function candidate needs to be defined to parameterize a variable-structure controller that guarantees asymptotic stability of the closed-loop system dynamics. Because $\dot{s} = 0$ has to be ensured in addition to $s = 0$, the definition

$$V^{\langle \mathrm{II} \rangle} = \frac{1}{2} \cdot \left(s^2 + \lambda \dot{s}^2 \right) \quad \text{with the scaling factor} \quad \lambda > 0 \tag{14}$$

is employed. Its time derivative results in

$$\begin{aligned} \dot{V}^{\langle \mathrm{II} \rangle} &= s \cdot \dot{s} + \lambda \cdot \dot{s} \cdot \ddot{s} \\ &= s \cdot \dot{s} + \dot{s} \cdot \left(-\frac{\lambda \gamma_0}{\gamma_1} \dot{s} + \frac{\lambda}{\gamma_1} \sum_{r=0}^{n} \alpha_{r-1} \tilde{\xi}_1^{(r)}(t) \right) < 0, \end{aligned} \tag{15}$$

where the special parameterization $\lambda = \gamma_1 > 0$ can be used without loss of generality. This is due to the fact that scaling of $\dot{V}^{\langle \mathrm{II} \rangle}$ in (15) can be performed by a suitable choice of γ_0 and α_r.

Using $\lambda = \gamma_1$ allows for simplifying the expression (15) under consideration of the control-dependent term $\tilde{\xi}^{(n)}(t) = \dot{x}_n(t) - x_{1,\mathrm{d}}^{(n)}(t) = u(t) - x_{1,\mathrm{d}}^{(n)}(t)$ according to

$$\dot{V}^{\langle \mathrm{II} \rangle} = s \cdot \dot{s} + \dot{s} \cdot \left(-\gamma_0 \dot{s} + \sum_{r=0}^{n-1} \alpha_{r-1} \tilde{\xi}_1^{(r)}(t) + \alpha_{n-1} \cdot \left(u(t) - x_{1,\mathrm{d}}^{(n)}(t) \right) \right) < 0. \tag{16}$$

As before, a conservative stabilization of the closed-loop system is desired that allows for a finite-time convergence toward $s = 0$. This can be achieved by setting

$$\dot{V}^{\langle \mathrm{II} \rangle} < -\eta_1 \cdot |\dot{s}| - \eta_2 \cdot |s| \cdot |\dot{s}| = -\dot{s} \cdot \operatorname{sign}(\dot{s}) \cdot (\eta_1 + \eta_2 \cdot |s|) \tag{17}$$

which finally leads to the nonlinear feedback controller [4, generalized form of Eqs. (22), (23)]

$$u(t) = u^{\langle \mathrm{II} \rangle}(t) = x_{1,\mathrm{d}}^{(n)}(t) + \frac{1}{\alpha_{n-1}} \cdot \left(\gamma_0 \dot{s} - s - \sum_{r=0}^{n-1} \alpha_{r-1} \tilde{\xi}_1^{(r)}(t) - \operatorname{sign}(\dot{s}) \cdot (\tilde{\eta}_1 + \tilde{\eta}_2 \cdot |s|) \right) \tag{18}$$

with $\tilde{\eta}_i \geq \eta_i > 0$ for both $i \in \{1, 2\}$.

2.2 Extension by One-Sided Barrier Lyapunov Functions

Both the control laws $u^{\langle \mathrm{I} \rangle}(t)$ and $u^{\langle \mathrm{II} \rangle}(t)$ can be extended by a one-sided barrier Lyapunov function approach in such a way that the generally time-varying strict state (respectively output) constraint

$$x_1(t) < \bar{x}_{1,\max}(t) := x_{1,\mathrm{d}}(t) + \Delta x_{1,\max}(t) \tag{19}$$

with $\Delta x_{1,\max}(t) > 0$ is guaranteed not to be violated for each point of time $t > 0$. Note that the initial conditions for the state vector $\mathbf{x}(t)$ at the point of time $t = 0$ have to be compatible with this constraint. Moreover, it is necessary that the sliding surface $s = 0$ for $x_1(t) = x_{1,\mathrm{d}}(t)$ lies within the admissible operating range that is defined by (19).

Then, the extended Lyapunov function ansatz

$$V^{\langle j,\mathrm{A} \rangle} = V^{\langle j \rangle} + V^{\langle \mathrm{A} \rangle} > 0 \quad \text{for} \quad s \neq 0 \tag{20}$$

with

$$V^{\langle \mathrm{A} \rangle} = \rho_{\mathrm{V}} \cdot \ln \left(\frac{\sigma_{\mathrm{V}} \cdot \bar{x}_{1,\max}(t)}{\bar{x}_{1,\max}(t) - x_1(t)} \right) \quad \text{and} \quad x_1(t) < \bar{x}_{1,\max}(t) \tag{21}$$

is introduced for both alternatives $j \in \{\mathrm{I}, \mathrm{II}\}$. In (21), the parameter $\rho_{\mathrm{V}} > 0$ needs to be chosen in such a way that the singularity $\bar{x}_{1,\max}(t) - x_1(t) = 0$ represents a repelling potential, where control constraints are not violated for usual operating conditions, and that the term $V^{\langle j \rangle}$ has dominating influence in the neighborhood of $s = 0$. In addition, the parameter $\sigma_{\mathrm{V}} > 0$ can be utilized to adapt the steepness of the barrier function near its singularity.

The time derivative of (20) can be computed as[1]

$$\dot{V}^{\langle j,\mathrm{A} \rangle} = \dot{V}^{\langle j \rangle} + \dot{V}^{\langle \mathrm{A} \rangle} < 0 \quad \text{with}$$

$$\dot{V}^{\langle \mathrm{A} \rangle} := \left(\frac{\partial V^{\langle \mathrm{A} \rangle}}{\partial \mathbf{x}} \right)^T \cdot \dot{\mathbf{x}}(t) = \frac{\rho_{\mathrm{V}}}{\bar{x}_{1,\max}(t)} \cdot \left(\frac{-x_1(t) \cdot \dot{\bar{x}}_{1,\max}(t) + \dot{x}_1(t) \cdot \bar{x}_{1,\max}(t)}{\bar{x}_{1,\max}(t) - x_1(t)} \right). \tag{22}$$

[1] Note that the expression $\dot{V}^{\langle \mathrm{A} \rangle}$ does not explicitly depend on the system input u in any of the applications considered in this chapter.

In analogy to the fundamental first-order sliding mode control law $u^{\langle \mathrm{I} \rangle}(t)$ derived from (8), the inequality

$$s \cdot \underbrace{\left(\sum_{r=0}^{n-2} \alpha_r \tilde{\xi}_1^{(r+1)}(t) + u(t) - x_{1,\mathrm{d}}^{(n)}(t) + \eta \cdot \operatorname{sign}(s) + \frac{1}{s} \cdot \dot{V}^{\langle \mathrm{A} \rangle} \right)}_{-\beta \cdot \operatorname{sign}(s)} < 0 \tag{23}$$

has to be fulfilled to prevent overshooting the state constraint (19) and to stabilize the error dynamics in a reliable way.

Under consideration of the term $u^{\langle \mathrm{I} \rangle}(t)$ defined in (9), the modified control law

$$u(t) = u^{\langle \mathrm{I,A} \rangle}(t) = u^{\langle \mathrm{I} \rangle}(t) - \frac{s}{s^2 + \tilde{\varepsilon}} \cdot \dot{V}^{\langle \mathrm{A} \rangle} \tag{24}$$

is obtained, in which the rational term $\frac{1}{s}$ in (23) has been approximated by the expression $\frac{s}{s^2+\tilde{\varepsilon}}$ with the small positive constant $\tilde{\varepsilon} > 0$. The approximation of this rational term ensures that the control law $u^{\langle \mathrm{I,A} \rangle}(t)$ is regular on the sliding surface $s = 0$ and that the barrier Lyapunov function becomes inactive as soon as the control goal has been reached. This is especially true in the case that interval uncertainty has a non-negligible influence on the system dynamics. This uncertainty leads to the fact that the sign of s can usually no longer be determined unambiguously in the close vicinity of $s = 0$. Hence, a good approximation of the rational term $\frac{1}{s}$ is only necessary for $|s| \gg 0$, where $\frac{1}{s} \approx \frac{s}{s^2+\tilde{\varepsilon}}$ holds.

For the special case of a time-independent state constraint $\bar{x}_{1,\max} = \text{const}$ with $\dot{\bar{x}}_{1,\max} = 0$, the control law (24) simplifies to

$$u(t) = u^{\langle \mathrm{I,A} \rangle}(t) = u^{\langle \mathrm{I} \rangle}(t) - \frac{s}{s^2 + \tilde{\varepsilon}} \cdot \rho_{\mathrm{V}} \cdot \left(\frac{x_2(t)}{\bar{x}_{1,\max} - x_1(t)} \right). \tag{25}$$

In a similar way, the second-order sliding mode control procedure can be extended by the barrier function (21). Following the same steps as in Eqs. (22)–(25) yields the control law

$$u(t) = u^{\langle \mathrm{II,A} \rangle}(t) = u^{\langle \mathrm{II} \rangle}(t) - \frac{1}{\alpha_{n-1}} \cdot \frac{\dot{s}}{\dot{s}^2 + \tilde{\varepsilon}} \cdot \dot{V}^{\langle \mathrm{A} \rangle}, \tag{26}$$

that can again be simplified as in (22) to obtain the control signal

$$u(t) = u^{\langle \mathrm{II,A} \rangle}(t) = u^{\langle \mathrm{II} \rangle}(t) - \frac{1}{\alpha_{n-1}} \cdot \frac{\dot{s}}{\dot{s}^2 + \tilde{\varepsilon}} \cdot \rho_{\mathrm{V}} \cdot \left(\frac{x_2(t)}{\bar{x}_{1,\max} - x_1(t)} \right) \tag{27}$$

for constant state constraints with $\dot{\bar{x}}_{1,\max} = 0$.

2.3 Extension by Two-Sided Barrier Lyapunov Functions

As for the case of one-sided state constraints, also two-sided barrier Lyapunov functions can be combined with the fundamental first- and second-order sliding mode controllers. For this purpose, the Lyapunov functions $V^{\langle j \rangle}$, $j \in \{\mathrm{I}, \mathrm{II}\}$, are extended by an additive term $V^{\langle \mathrm{B} \rangle}$ according to

$$V^{\langle j,\mathrm{B} \rangle} = V^{\langle j \rangle} + V^{\langle \mathrm{B} \rangle} > 0 \quad \text{for} \quad s \neq 0. \tag{28}$$

In (28), the additive term $V^{\langle \mathrm{B} \rangle}$ can either be chosen to avoid state deviations $\left| x_1(t) - x_{1,\mathrm{d}}(t) \right| \geq \bar{\chi}$ or to avoid large tracking errors with $|s(t)| \geq \bar{\chi}$. In this contribution, only the second option is considered, where $\bar{\chi}$ is assumed to be constant. Note that all corresponding equations can be generalized in a straightforward manner to the first option as well and to the case of time-dependent bounds $\bar{\chi}(t)$.

Penalizing errors with respect to the absolute value of s leads to the definition

$$V^{\langle \mathrm{B} \rangle} = \rho_{\mathrm{V}} \cdot \ln\left(\frac{\bar{\chi}^{2l}}{\bar{\chi}^{2l} - s^{2l}} \right) \quad \text{with} \quad l \in \mathbb{N} \tag{29}$$

and the even powers $2l$, enforcing symmetric bounds for the sliding variable s. Increasing values for l typically lead to the fact that resulting state trajectories come closer to the edges of the admissible operating range.

The time derivative of (29) is then given by

$$\dot{V}^{\langle \mathrm{B} \rangle} = \left(\frac{\partial V^{\langle \mathrm{B} \rangle}}{\partial \mathbf{x}} \right)^T \cdot \dot{\mathbf{x}} = \rho_{\mathrm{V}} \cdot \frac{2l \cdot s^{2l-1} \dot{s}}{\bar{\chi}^{2l} - s^{2l}}. \tag{30}$$

According to the previous subsections, the requirement $\dot{V}^{\langle j,\mathrm{B} \rangle} < 0$ for $s \neq 0$ (and $\dot{s} \neq 0$, resp.) leads to the control laws

$$u^{\langle \mathrm{I},\mathrm{B} \rangle}(t) = u^{\langle \mathrm{I} \rangle}(t) - \frac{1}{s} \cdot \dot{V}^{\langle \mathrm{B} \rangle} = u^{\langle \mathrm{I} \rangle}(t) - \rho_{\mathrm{V}} \cdot \frac{2l \cdot s^{2l-2} \dot{s}}{\bar{\chi}^{2l} - s^{2l}} \tag{31}$$

in the case of the first-order sliding mode or to

$$u^{\langle \mathrm{II},\mathrm{B} \rangle}(t) = u^{\langle \mathrm{II} \rangle}(t) - \frac{1}{\alpha_{n-1}} \cdot \frac{1}{\dot{s}} \cdot \dot{V}^{\langle \mathrm{B} \rangle} = u^{\langle \mathrm{II} \rangle}(t) - \frac{1}{\alpha_{n-1}} \cdot \rho_{\mathrm{V}} \cdot \frac{2l \cdot s^{2l-1}}{\bar{\chi}^{2l} - s^{2l}} \tag{32}$$

for the second-order sliding mode. To preserve the additive superposition of a control $u^{\langle \mathrm{I} \rangle}(t)$ with a correction term resulting from the barrier function as in (24) and (25), the term $\dot{s}$ is typically estimated by a suitable low-pass filtered differentiation or by means of an observer for the implementation of (31).

2.4 Interval Extensions of Sliding Mode Control Strategies

To guarantee asymptotic stability despite bounded uncertainty in system parameters $\mathbf{p}$, it is possible to apply interval techniques in real time for the implementation of the before-mentioned sliding mode control approaches [21]. The fundamental prerequisite for the applicability of interval techniques is that all parameters (and a priori unknown disturbances as well as measurement and state reconstruction errors) are bounded by closed interval vectors $[\mathbf{p}]$ that are defined component-wise according to $\mathbf{p} \in [\mathbf{p}] = \left[\underline{\mathbf{p}};\ \overline{\mathbf{p}}\right]$ with $\underline{p}_i \leq p_i \leq \overline{p}_i, i \in \{1, \ldots, n_\mathrm{p}\}$. Furthermore, it is assumed that the dynamic systems are given as nth-order sets of ordinary differential equations (ODEs)

$$\begin{bmatrix} \dot{x}_1(t) \\ \dot{x}_2(t) \\ \vdots \\ \dot{x}_{n-1}(t) \\ \dot{x}_n(t) \end{bmatrix} = \begin{bmatrix} x_2(t) \\ x_3(t) \\ \vdots \\ x_n(t) \\ a\left(\mathbf{x}(t), \mathbf{p}\right) + b\left(\mathbf{x}(t), \mathbf{p}\right) \cdot u(t) \end{bmatrix} \tag{33}$$

in nonlinear controller canonical form. These ODEs are a natural generalization of the pure integrator chain in Eq. (1). Note that a suitable nonlinear coordinate transformation of the fuel cell model in Sect. 4 leads exactly to this type of system structure.

For the control synthesis it is assumed as before that the system output is given by the first state variable according to

$$y(t) = x_1(t) \tag{34}$$

and that all state variables are known at each point of time in terms of guaranteed interval bounds $\mathbf{x}(t) \in [\mathbf{x}](t) = \left[\underline{\mathbf{x}}(t);\ \overline{\mathbf{x}}(t)\right]$.

For the sake of controllability (and, therefore, also for the existence of the following generalized control laws), it has to be guaranteed that

$$0 \notin b\left([\mathbf{x}](t), [\mathbf{p}]\right) := \left\{ b\left(\mathbf{x}(t), \mathbf{p}\right) | b\left(\mathbf{x}(t), \mathbf{p}\right) \text{ for all } \mathbf{x}(t) \in [\mathbf{x}](t), \mathbf{p} \in [\mathbf{p}] \right\} \tag{35}$$

holds.

These assumptions lead to the possibility to define the output tracking error and its rth derivative by the interval expression

$$\tilde{\xi}_1^{(r)}(t) \in \left[\tilde{\xi}_1^{(r)}\right](t) = \left[x_1^{(r)}\right](t) - x_{1,\mathrm{d}}^{(r)}(t) \tag{36}$$

for each $r \in \{0, 1, \ldots, n\}$. Furthermore, these tracking errors can be used to generalize the first-order sliding mode control laws according to

$$\left[u^{\langle \mathrm{I} \rangle}\right](t) = \frac{-a\left([\mathbf{x}](t), [\mathbf{p}]\right) + x_{1,\mathrm{d}}^{(n)}(t) - \sum_{r=0}^{n-2} \alpha_r \cdot \left[\tilde{\xi}_1^{(r+1)}\right](t) - \tilde{\eta} \cdot \operatorname{sign}([s])}{b\left([\mathbf{x}](t), [\mathbf{p}]\right)}, \tag{37}$$

$$\left[u^{\langle \mathrm{I,A} \rangle}\right](t) = \left[u^{\langle \mathrm{I} \rangle}\right](t) - \frac{1}{b\left([\mathbf{x}](t), [\mathbf{p}]\right)} \cdot \frac{[s]}{[s]^2 + \tilde{\varepsilon}} \cdot \left[\dot{V}^{\langle \mathrm{A} \rangle}\right](t), \tag{38}$$

and

$$\left[u^{\langle \mathrm{I,B} \rangle}\right](t) = \left[u^{\langle \mathrm{I} \rangle}\right](t) - \frac{1}{b\left([\mathbf{x}](t), [\mathbf{p}]\right)} \cdot \rho_{\mathrm{V}} \cdot \frac{2l\,[s]^{2l-2}\,[\dot{s}]}{\bar{\chi}^{2l} - [s]^{2l}}. \tag{39}$$

Similarly, the interval-based generalization for the second-order sliding mode approach is given either by

$$\left[u^{\langle \mathrm{II} \rangle}\right](t) = \frac{-a\left([\mathbf{x}](t), [\mathbf{p}]\right) + x_{1,\mathrm{d}}^{(n)}(t) + \frac{1}{\alpha_{n-1}} \cdot \left[\tilde{v}^{\langle \mathrm{II} \rangle}\right](t)}{b\left([\mathbf{x}](t), [\mathbf{p}]\right)} \tag{40}$$

with

$$\left[\tilde{v}^{\langle \mathrm{II} \rangle}\right](t) := \left(\gamma_0 \cdot [\dot{s}] - [s] - \sum_{r=0}^{n-1} \alpha_{r-1} \cdot \left[\tilde{\xi}_1^{(r)}\right](t) - \operatorname{sign}([\dot{s}]) \cdot (\tilde{\eta}_1 + \tilde{\eta}_2 \cdot |[s]|)\right), \tag{41}$$

$$\left[u^{\langle \mathrm{II,A} \rangle}\right](t) = \left[u^{\langle \mathrm{II} \rangle}\right](t) - \frac{1}{b\left([\mathbf{x}](t), [\mathbf{p}]\right)} \cdot \frac{1}{\alpha_{n-1}} \cdot \frac{[\dot{s}]}{[\dot{s}]^2 + \tilde{\varepsilon}} \cdot \left[\dot{V}^{\langle \mathrm{A} \rangle}\right](t), \tag{42}$$

or by

$$\left[u^{\langle \mathrm{II,B} \rangle}\right](t) = \left[u^{\langle \mathrm{II} \rangle}\right](t) - \frac{1}{b\left([\mathbf{x}](t), [\mathbf{p}]\right)} \cdot \frac{1}{\alpha_{n-1}} \cdot \rho_{\mathrm{V}} \cdot \frac{2l\,[s]^{2l-1}}{\bar{\chi}^{2l} - [s]^{2l}}. \tag{43}$$

The choice between these different options is made as before in dependence of the type of barrier function to be taken into account by the robust control synthesis. Furthermore, the expressions $a\left([\mathbf{x}](t), [\mathbf{p}]\right)$, $b\left([\mathbf{x}](t), [\mathbf{p}]\right)$, $\left[\dot{V}^{\langle \mathrm{A} \rangle}\right](t)$, $[s] := [s](t)$, and $[\dot{s}] := [\dot{s}](t)$ denote the interval-dependent evaluations of the corresponding entries of the state equations, the time derivatives of the barrier function, the sliding surface, and its time derivative, respectively.

For the actual control implementation in a real-time environment, the interval expressions mentioned above are evaluated by means of the C++ toolbox C-XSC [13]. To guarantee asymptotic stability for all possible operating conditions, the corresponding interval variables have to be chosen in such a way that they include the state and parameter uncertainties in a rigorous way. Assuming a quasi-continuous implementation, in which the effect of time discretization errors is negligibly small, the final control signal $u(t)$ needs to be chosen from the previous intervals in such

a way that it guarantees asymptotic stability regardless of the sign of $b(\mathbf{x}(t), \mathbf{p})$, $0 \notin b([\mathbf{x}](t), [\mathbf{p}])$.

For this reason, the set of possible control variables, guaranteeing a minimum signal amplitude, consists of the infima and the suprema of the before-mentioned interval-valued control strategies. These values are given as $\underline{u} := \inf\{[u]\}$ and $\overline{u} := \sup\{[u]\}$, respectively, where $[u]$ is either of the control laws (37)–(40), (42), or (43). To account for roundoff and representation errors, the infima and suprema are inflated by a small positive value $\varepsilon > 0$ to obtain the final set of control candidates

$$\mathcal{U} := \left\{\underline{u} - \varepsilon, \underline{u} + \varepsilon, \overline{u} - \varepsilon, \overline{u} + \varepsilon\right\}. \tag{44}$$

From this set, the control (with minimum absolute value) is chosen, which guarantees to satisfy the inequality $\dot{V} < 0$ (or its generalization for the barrier Lyapunov function approach) despite the considered interval uncertainty.

2.5 Illustrative Simulation Examples

In this section, an illustrative benchmark example is used to visualize the effectiveness of the before-mentioned fundamental sliding mode control approaches and their interval-based extensions. The considered system model with $n = 3$ is given as

$$\begin{bmatrix} \dot{x}_1(t) \\ \dot{x}_2(t) \\ \dot{x}_3(t) \end{bmatrix} = \begin{bmatrix} x_2(t) \\ x_3(t) \\ p_1 x_1 + p_2 x_2 + p_3 x_3 + p_4 u(t) \end{bmatrix} \tag{45}$$

with

(a) the nominal parameters $p_1 = p_2 = p_3 = 0$ and $p_4 = 1$ as well as
(b) the uncertain parameters $p_i \in [-0.1;\ 0.1]$, $i \in \{1, 2, 3\}$, and $p_4 = 1$.

This system model corresponds to the dynamics of a point mass (position $x_1(t)$, velocity $x_2(t)$) and a normalized input force $x_3(t)$, where the underlying actuator dynamics with the control input $u(t)$ are characterized by both the nominal and uncertain parameters p_j, $j \in \{1, \ldots, 4\}$.

In all simulations, the desired reference trajectory is given by

$$x_{1,\mathrm{d}}(t) = 1 - e^{-t}\ ,\quad t \geq 0, \tag{46}$$

with the initial system states $\mathbf{x}(0) = \mathbf{0}$. Note that these initial states do not satisfy the sliding condition $s = 0$ at the initial point of time $t = 0$. Hence, even without uncertainty, there exists a transition between the reaching and sliding phase.

A summary of the selected system parameters as well as of the parameterization of the Lyapunov function candidates and the corresponding barrier functions is given for all considered simulation scenarios in Table 1. For the sake of simplicity, it is assumed

Table 1 Parameterization of sliding mode control approaches for the considered benchmark application

Scenario	Definition of Lyapunov function V	Barrier	System parameters	Measurement tolerance for x_1	Parameters of s	Variable-structure gains
Case 1	$V^{\langle \mathrm{I} \rangle}$	–	$p_1 = p_2 = p_3 = 0$, $p_4 = 1$	–	$\alpha_0 = 1, \alpha_1 = 0.9$	$\tilde{\eta} = 20$
Case 2	$V^{\langle \mathrm{I,A} \rangle}$	$\rho_\mathrm{V} = 0.5, \sigma_\mathrm{V} = 1$, $\Delta x_{1,\max} = 0.01$	$p_1 = p_2 = p_3 = 0$, $p_4 = 1$	–	$\alpha_0 = 1, \alpha_1 = 0.9$	$\tilde{\eta} = 20$
Case 3	$V^{\langle \mathrm{I,A} \rangle}$	$\rho_\mathrm{V} = 0.75, \sigma_\mathrm{V} = 1$, $\Delta x_{1,\max} = 0.01$	$p_i \in [-0.1;\ 0.1]$, $i = \{1, 2, 3\}$, $p_4 = 1$	$0.0025 \cdot [-1;\ 1]$	$\alpha_0 = 15, \alpha_1 = 0.9$	$\tilde{\eta} = 20$
Case 4	$V^{\langle \mathrm{II} \rangle}$	–	$p_1 = p_2 = p_3 = 0$, $p_4 = 1$	–	$\alpha_{-1} = 0.01, \alpha_0 = 1$, $\alpha_1 = 0.9, \alpha_2 = 1$, $\gamma_0 = 1, \gamma_1 = 10$	$\tilde{\eta}_1 = \tilde{\eta}_2 = 20$
Case 5	$V^{\langle \mathrm{II,A} \rangle}$	$\rho_\mathrm{V} = 0.02, \sigma_\mathrm{V} = 1$, $\Delta x_{1,\max} = 0.01$	$p_1 = p_2 = p_3 = 0$, $p_4 = 1$	–	$\alpha_{-1} = 0.01, \alpha_0 = 1$, $\alpha_1 = 0.9, \alpha_2 = 1$, $\gamma_0 = 1, \gamma_1 = 10$	$\tilde{\eta}_1 = \tilde{\eta}_2 = 20$
Case 6	$V^{\langle \mathrm{II,B} \rangle}$	$\rho_\mathrm{V} = 0.5$, $\bar{\chi} = 5{\cdot}10^{-6}, l = 5$	$p_1 = p_2 = p_3 = 0$, $p_4 = 1$	–	$\alpha_{-1} = 0.1, \alpha_0 = 1$, $\alpha_1 = 0.9, \alpha_2 = 1$, $\gamma_0 = 1, \gamma_1 = 10$	$\tilde{\eta}_1 = \tilde{\eta}_2 = 20$
Case 7	$V^{\langle \mathrm{II} \rangle}$	–	$p_1 = p_2 = p_3 = 0$, $p_4 = 1$	–	$\alpha_{-1} = 0.01, \alpha_0 = 10$, $\alpha_1 = 0.9, \alpha_2 = 0.1$, $\gamma_0 = 1, \gamma_1 = 10$	$\tilde{\eta}_1 = \tilde{\eta}_2 = 20$
Case 8	$V^{\langle \mathrm{II} \rangle}$	–	$p_1 = p_2 = p_3 = 0$, $p_4 = 1$	–	$\alpha_{-1} = 0.01, \alpha_0 = 1$, $\alpha_1 = 0.9, \alpha_2 = 1$, $\gamma_0 = 1, \gamma_1 = 10$	$\tilde{\eta}_1 = \tilde{\eta}_2 = 0$
Case 9	$V^{\langle \mathrm{II} \rangle}$	–	$p_1 = p_2 = p_3 = 0$, $p_4 = 1$	–	$\alpha_{-1} = 0.01, \alpha_0 = 10$, $\alpha_1 = 0.9, \alpha_2 = 0.1$, $\gamma_0 = 1, \gamma_1 = 10$	$\tilde{\eta}_1 = \tilde{\eta}_2 = 0$

in the non-interval implementations (Cases 1 and 2 for the first-order sliding mode) that all states $\mathbf{x}(t)$ can be measured accurately for the quasi-continuous sliding mode implementation. This simplifying assumption is removed in the simulation Case 3 and in the further course of this contribution for the application of sliding mode techniques to the temperature control of a high-temperature SOFC system.

For both the first- and second-order sliding mode controllers $u^{\langle \mathrm{I} \rangle}(t)$ and $u^{\langle \mathrm{II} \rangle}(t)$, the parameters of the sliding surface are chosen purposefully in such a way that the roots of the associated characteristic polynomial, corresponding to

$$\sum_{r=0}^{n-1} \alpha_r \zeta^r = \alpha_0 + \alpha_1 \zeta + \zeta^2 = 0 \tag{47}$$

in the first-order case, are conjugate complex. In such a way, the straightforward sliding mode implementation without state barriers leads to an oscillatory behavior in the reaching phase with overshooting the reference trajectory $x_{1,\mathrm{d}}(t)$, see the Cases 1 and 4 as well as Figs. 1 and 2.

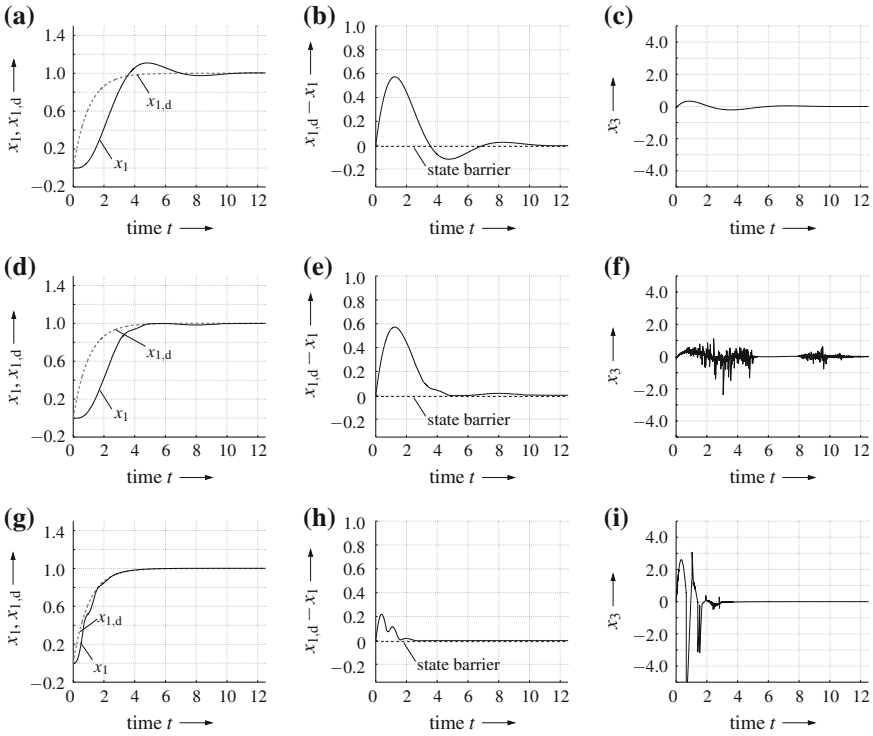

Fig. 1 Simulation results for the benchmark application with first-order sliding mode techniques. **a** System output (Case 1). **b** Tracking error (Case 1). **c** State x_3 (Case 1). **d** System output (Case 2). **e** Tracking error (Case 2). **f** State x_3 (Case 2). **g** System output (Case 3). **h** Tracking error (Case 3). **i** State x_3 (Case 3)

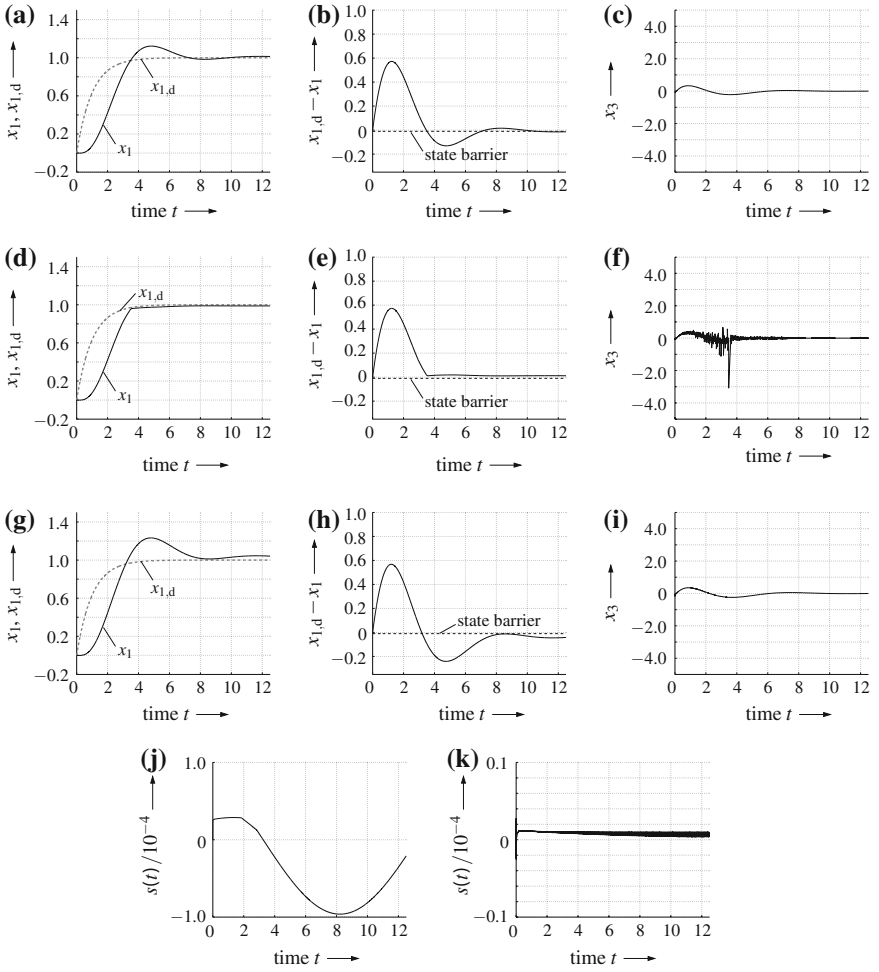

Fig. 2 Simulation results for the benchmark application with second-order sliding mode (part 1). **a** System output (Case 4). **b** Tracking error (Case 4). **c** State x_3 (Case 4). **d** System output (Case 5). **e** Tracking error (Case 5). **f** State x_3 (Case 5). **g** System output (Case 6). **h** Tracking error (Case 6). **i** State x_3 (Case 6). **j** Variation of $s(t)$ (Case 4). **k** Variation of $s(t)$ (Case 6)

Introducing a strict time-varying barrier for the state $x_1(t)$ according to (19) in the Cases 2 and 5 helps to reliably avoid the overshoot. This holds for both the first- and second-order sliding mode controllers with $u(t) = u^{\langle \mathrm{I,A} \rangle}(t)$ and $u(t) = u^{\langle \mathrm{II,A} \rangle}(t)$.

In addition to using the state barrier according to (19), the two-sided constraint (29) is employed in the Case 6 with $u(t) = u^{\langle \mathrm{II,B} \rangle}(t)$. Generally, the results for the first- and second-order cases show the same behavior. Subsequently, only the second-order result is depicted because it highlights the advantage of the extension $V^{\langle \mathrm{B} \rangle}$ more clearly for the considered application scenario: Although the two-sided barrier

extension $V^{\langle \mathrm{B} \rangle}$ according to (28) does not allow for limiting the range of state variables explicitly, it allows for limiting the deviations of states from the sliding surface s in a reliable way. This limits the variable-structure control amplitudes for the Case 6, where fixed gains $\tilde{\eta}_1$ and $\tilde{\eta}_2$ are coupled with the absolute value of s in a multiplicative way. It has to be pointed out that the maximum admissible deviation $\bar{\chi}$ as well as the necessary order l in the barrier term $V^{\langle \mathrm{B} \rangle}$ have to be chosen carefully to make sure that the admissible operating range is not violated. This may happen for specifying too tight operating ranges that inevitably lead to large control amplitudes. Such large amplitudes may, on the one hand, not be compatible with actuator constraints in a real-life application. On the other hand, they may also lead to violations of the admissible operating range if too large integration step sizes (resp. sampling times) are specified for the numerical evaluation of the system ODEs in a quasi-continuous control implementation. Especially due to the latter issue, future work will deal with the direct consideration of time discretization phenomena within the sliding mode design for continuous-time dynamic systems. Note that violations of barrier terms—due to time discretization effects in a regularized control implementation that ensures finite control values in the second-order case (the same holds for the one-sided barrier functions)—lead to nonlinear integrator wind-up phenomena in the computation of $s(t)$ and $\tilde{\xi}^{(-1)}(t)$. These wind-up effects have to be avoided by suitable parameterizations since their presence inevitably deteriorates the control quality.

The robustness of the interval-based control extensions presented in Sect. 2.4 is confirmed in the extended simulations in Case 3. It can be seen that the application of the fundamental interval-based control approach (37) guarantees asymptotic stability of the closed-loop dynamics after a careful setting of the controller's parameters. Here, uncertainties in the system parameters p_j as well as additive bounded errors in the measured state $x_1(t)$ were considered.

Note that the choice of $\Delta x_{1,\max}$ must be made in such a way that the sliding surface is reachable despite the above-mentioned measurement errors for $x_1(t)$. Due to the fact that the state barrier $\bar{x}_{1,\max}(t)$ is only considered explicitly in the Cases 2, 3, and 5, the violation of this constraint is obvious in all remaining scenarios.

Simulation results for $V^{\langle \mathrm{II,A} \rangle}$ are not presented due to an identical behavior as in Case 3. Note that the use of the second-order sliding mode is not advantageous for the case of interval uncertainty with large diameters that are directly included in the expression (11). Then, a definite statement about the signs of s and $\dot{s}$ may no longer be possible. Although the second-order sliding mode control approach leads to more smooth control signals than the first-order one for the non-interval case, this advantageous filtering property is lost as soon as ambiguities in the signs of s and $\dot{s}$ arise. Therefore and due to the fact that the uncertain parameters in the following sections have a large influence, interval-based implementations currently focus on first-order sliding mode techniques. Extensions to higher-order cases and toward an improved systematic parameterization of interval-based control approaches are subjects of ongoing work.

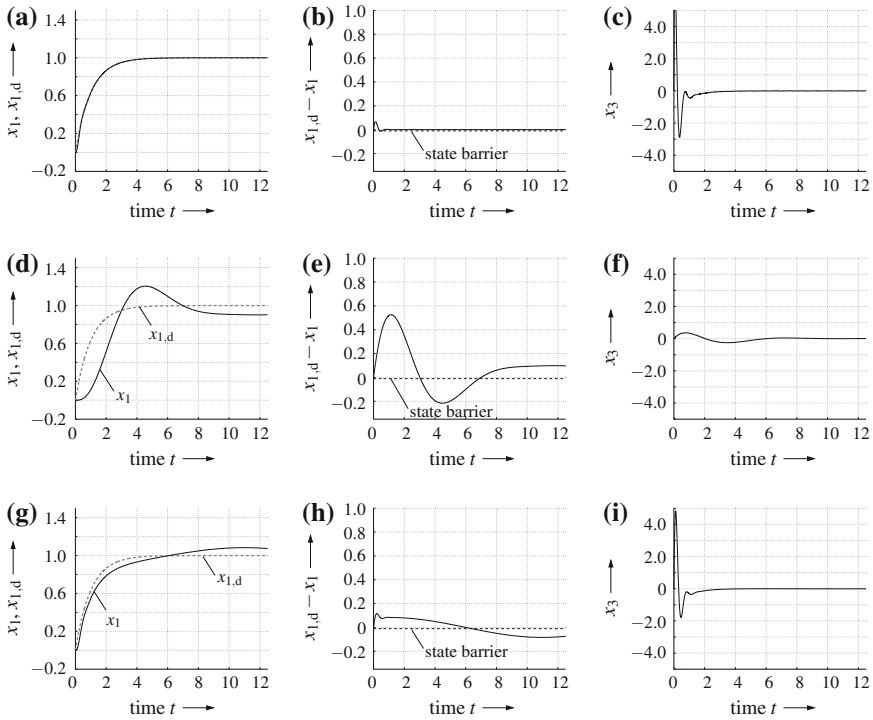

Fig. 3 Simulation results for the benchmark application with second-order sliding mode (part 2). **a** System output (Case 7). **b** Tracking error (Case 7). **c** State x_3 (Case 7). **d** System output (Case 8). **e** Tracking error (Case 8). **f** State x_3 (Case 8). **g** System output (Case 9). **h** Tracking error (Case 9). **i** State x_3 (Case 9)

A detailed investigation of the influence of the parameters of the sliding surface with and without variable-structure control parts can be found in Fig. 3 (Cases 7–9). In general, increased gain values α_0 lead to smaller tracking errors. However, accurate trajectory tracking is only possible when the variable-structure part is active. The same also holds in an analogous manner for the first-order sliding mode.

3 Control-Oriented SOFC Modeling

As described, for example, in [3, 10, 18, 33], SOFCs are characterized by a nonlinear dynamic behavior if large domains are considered for the temperature operating point as well as for the electric load of the system. Focusing on the temperature distribution in the interior of high-temperature fuel cell stack modules, the corresponding dynamics can be described by sets of partial differential equations. The goal of control design for SOFC systems is to prevent local over-temperatures in the

interior of the fuel cell stack module by a suitable actuation of the gas preheaters. This helps to reduce mechanical strain of the SOFC components due to different thermal expansion properties and thus avoids accelerated aging or in the worst case the destruction of the SOFC. The control task consists in varying the enthalpy flow provided to the fuel cell stack by changes in the temperature of the preheated gases and by variations of the gas mass flows. Typically, only the enthalpy flow of the cathode gas is used for this purpose, while the anode gas mass flow is employed to specify the electric power that can be produced by the system.

However, system models given by partial differential equations are often too complex to design controllers and state estimators that can be implemented in real time. Therefore, a control-oriented modeling procedure is used in the following to approximate the system dynamics by a finite-dimensional set of ODEs. For such systems of ODEs, the design of feedforward as well as feedback controllers can be performed by state-of-the-art approaches. Classically, this is done in the frame of SOFC systems by (gain-scheduled) PI (proportional, integral) controllers as well as by linear model-predictive control techniques [10, 34]. Since the applicability of these techniques requires that the operating temperature of the SOFC stack does not deviate too far from the point at which the nonlinear system model is linearized for design purposes, they may not be well suited if larger operating domains are considered in a flexible future power supply grid. Moreover, the use of classical linear control approaches requires an accurate knowledge of the parameters of the describing sets of ODEs. However, parameters such as heat conductivities of the fuel cell material and specific heat capacities of the fuel gases are uncertain and cannot be identified experimentally with absolute accuracy. Hence, robust control procedures have to handle such uncertainties in a reliable way. For this reason, interval-based sliding mode procedures [21, 27] are extended in this contribution to implement robust control strategies under state, input, and input rate constraints.

The prerequisite for this type of control design is the derivation of control-oriented system models. These models are derived from a spatial semi-discretization of the SOFC stack which consists of a finite number of planar fuel cells in electric series connection. The fuel cell stack is constructed in such a way that the electric current through the individual cells is orthogonal to the gas mass flow. The control-oriented model, described in detail in [27], assumes that all dynamic variables are spatially homogeneous over finitely large domains. This homogeneity assumption holds for the stack module temperatures, the electric currents as well as the corresponding internal gas mass flows. In such a way, thermodynamic quantities such as heat conductivities and specific heat capacities represent effective quantities holding in an integral balance for each of the finite volume elements.

After setting up a parameterizable set of ODEs for the thermal behavior of the SOFC stack, the parameters were identified experimentally in previous work either by local or global optimization procedures. Note that the semi-discretization procedure is based on integral heat flow and energy balances for each of the finite volume elements $\mathcal{I}$ in the stack that is depicted in Fig. 4.

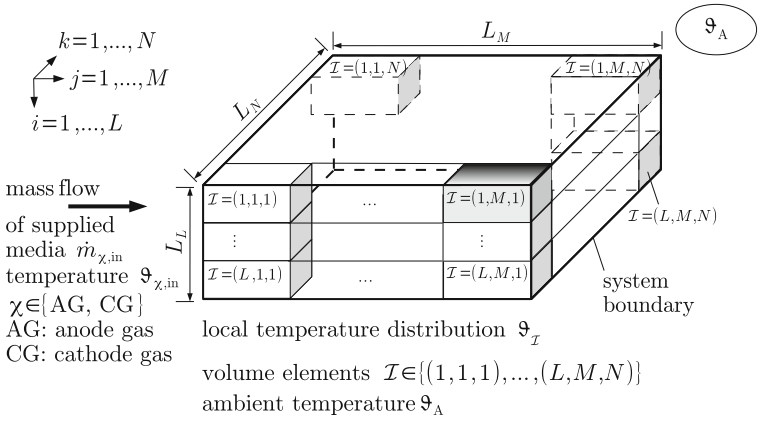

Fig. 4 Spatial semi-discretization of the SOFC stack

These integral heat flow balances lead to the ODEs

$$\dot{\vartheta}_\mathcal{I}(t) = \frac{\dot{Q}^\mathcal{I}_\text{HT}(t) + \sum_\text{G} \dot{Q}^\mathcal{I}_{\text{G},\mathcal{I}_j^-}(t) + \dot{Q}^\mathcal{I}_\text{EL}(t) + \dot{Q}^\mathcal{I}_\text{R}(t)}{c_\mathcal{I} m_\mathcal{I}} \tag{48}$$

for the temperature $\vartheta_\mathcal{I}(t)$ in each volume element $\mathcal{I}$, where the index $\text{G} \in \{\text{AG, CG}\}$ denotes the anode gas (AG) and the cathode gas (CG). For the test rig, available at the Chair of Mechatronics at the University of Rostock, the AG consists of a mixture of hydrogen (H_2), nitrogen (N_2), and water vapor (H_2O) which are jointly heated in the electric AG preheater. The CG is further given as a preheated flow of air. Additional parameters in (48) are the heat capacity $c_\mathcal{I}$ of the volume element $\mathcal{I}$ and its local mass parameter $m_\mathcal{I}$.

The heat flow term

$$\begin{aligned}\dot{Q}^\mathcal{I}_\text{HT}(t) = {} & \dot{Q}^\mathcal{I}_{\text{HT},\mathcal{I}_i^-}(t) + \dot{Q}^\mathcal{I}_{\text{HT},\mathcal{I}_i^+}(t) + \dot{Q}^\mathcal{I}_{\text{HT},\mathcal{I}_j^-}(t) \\ & + \dot{Q}^\mathcal{I}_{\text{HT},\mathcal{I}_j^+}(t) + \dot{Q}^\mathcal{I}_{\text{HT},\mathcal{I}_k^-}(t) + \dot{Q}^\mathcal{I}_{\text{HT},\mathcal{I}_k^+}(t)\end{aligned} \tag{49}$$

in (48) consists of heat transport between directly neighboring volume elements as well as heat transfer to the ambiance. In (49), the heat flows

$$\dot{Q}^\mathcal{I}_{\text{HT},\mathcal{J}}(t) = \beta^\mathcal{I}_\mathcal{J} \cdot (\vartheta_\mathcal{J}(t) - \vartheta_\mathcal{I}(t)) \tag{50}$$

are assumed to be directed from the volume elements $\mathcal{J} \in \{\mathcal{I}_i^-, \mathcal{I}_i^+, \mathcal{I}_j^-, \mathcal{I}_j^+, \mathcal{I}_k^-, \mathcal{I}_k^+\}$ into the element $\mathcal{I}$. Here, the coefficient $\beta^\mathcal{I}_\mathcal{J}$ is either the effective parameter for heat conduction in the interior of the fuel cell or the convective heat transfer coefficient (containing radiation effects in a locally linearized form) between the ambient medium and the elements at the stack boundary.

In detail, the index set $\mathcal{J}$ consists of the following entries: $\mathcal{I}_i^- := (i-1, j, k)$, $\mathcal{I}_i^+ := (i+1, j, k)$, $\mathcal{I}_j^- := (i, j-1, k)$, $\mathcal{I}_j^+ := (i, j+1, k)$, $\mathcal{I}_k^- := (i, j, k-1)$, and $\mathcal{I}_k^+ := (i, j, k+1)$. The temperatures $\vartheta_{\mathcal{I}_i^-}(t)$ and $\vartheta_{\mathcal{I}_i^+}(t)$ denote stack temperatures for $i \geq 2$ and $i \leq L-1$. The same holds for $\vartheta_{\mathcal{I}_j^-}(t)$ and $\vartheta_{\mathcal{I}_j^+}(t)$ with $j \geq 2$ and $j \leq M-1$ and for $\vartheta_{\mathcal{I}_k^-}(t)$ and $\vartheta_{\mathcal{I}_k^+}(t)$ with $k \geq 2$ and $k \leq N-1$. In all other cases, the values $\vartheta_{\mathcal{J}}(t)$ are set to the ambient temperature $\vartheta_{\mathrm{A}}(t) = \text{const}$.

In addition to these internal effects, the total enthalpy flow

$$\sum_{\mathrm{G}} \dot{Q}^{\mathcal{I}}_{\mathrm{G},\mathcal{I}_j^-}(t)\,, \quad \mathrm{G} \in \{\mathrm{AG}, \mathrm{CG}\}, \tag{51}$$

of AG and CG is included in the ODEs, where the mass flow $\dot{m}_{\mathrm{CG}}$ and its desired temperature $\vartheta_{\mathrm{CG,d}}$ are used to design a guaranteed stabilizing control strategy. Ohmic heat production $\dot{Q}^{\mathcal{I}}_{\mathrm{EL}}(t)$ and heat flows $\dot{Q}^{\mathcal{I}}_{\mathrm{R}}(t)$ due to an exothermic reaction between AG and CG conclude the energy balance. Detailed models for the local variations of the reacting gas mass flows and their temperature-dependent parameterizations as well as explicit expressions for the reaction enthalpies are given in [27].

The finite volume model from (48)–(51) is coupled with the dynamics of the AG and CG preheaters according to Fig. 5. As shown in [27, 28], it is essential to account for the preheater dynamics during the control design for non-stationary operating conditions to avoid unnecessary chattering of the system inputs.

According to [28], each preheater is described by two sets of first-order ODEs ($\mathrm{G} \in \{\mathrm{AG}, \mathrm{CG}\}$, $\chi \in \{\mathrm{H_2}, \mathrm{N_2}, \mathrm{H_2O}, \mathrm{CG}\}$)

$$T_{\mathrm{G}} \cdot \dot{v}_{\chi}(t) + v_{\chi}(t) + \tilde{d}_{\chi}(t) = v_{\chi,\mathrm{d}}(t) = \vartheta_{\chi,\mathrm{d}}(t) \cdot \dot{m}_{\chi,\mathrm{d}}(t) \tag{52}$$

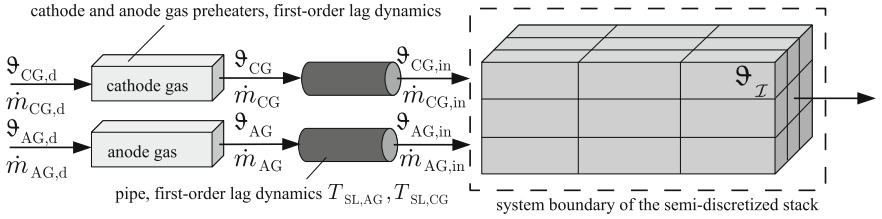

$\vartheta_{\mathrm{AG,d}}, \vartheta_{\mathrm{CG,d}}$	- desired values for temperatures of anode and cathode gas
$\vartheta_{\mathrm{AG,in}}, \vartheta_{\mathrm{CG,in}}$	- temperature of anode and cathode gas in the inlet gas manifold
$\vartheta_{\mathrm{AG}}, \vartheta_{\mathrm{CG}}$	- temperatures of anode and cathode gas at the preheater outlet
$\dot{m}_{\mathrm{AG}}, \dot{m}_{\mathrm{CG}}$	- measured mass flows of anode and cathode gas at the preheater outlet
$\dot{m}_{\mathrm{AG,d}}, \dot{m}_{\mathrm{CG,d}}$	- desired mass flows of anode and cathode gas
$T_{\mathrm{AG}}, T_{\mathrm{CG}}$	- time constants of the first-order lag dynamics of the preheaters

Fig. 5 Semi-discretization of the fuel cell stack module with gas preheaters

and

$$T_{\mathrm{SL,G}} \cdot \frac{\dot{v}_{\chi,\mathrm{in}}(t)}{L \cdot N} + \frac{v_{\chi,\mathrm{in}}(t)}{L \cdot N} = \frac{v_{\chi}(t)}{L \cdot N} = \frac{\vartheta_{\chi}(t) \cdot \dot{m}_{\chi}(t)}{L \cdot N} \tag{53}$$

with

$$v_{\chi,\mathrm{in}}(t) := \vartheta_{\chi,\mathrm{in}}(t) \cdot \dot{m}_{\chi,\mathrm{in}}(t) \quad \text{and} \quad \dot{m}_{\chi,\mathrm{d}} = \dot{m}_{\chi} = \dot{m}_{\chi,\mathrm{in}} \tag{54}$$

as well as the time constants T_{G} for the subsidiary temperature control and $T_{\mathrm{SL,G}}$ for the lag behavior due to transport phenomena in the gas supply lines (SL) between the preheaters and the SOFC stack.

In (52) and (53), the desired preheater temperatures (index d, serving as control inputs in addition to the desired mass flows $\dot{m}_{\mathrm{G,d}}$), are given by

$$\vartheta_{\chi,\mathrm{d}}(t) = \begin{cases} \vartheta_{\mathrm{AG,d}}(t) & \text{for } \chi \in \{\mathrm{H_2}, \mathrm{N_2}, \mathrm{H_2O}\} \\ \vartheta_{\mathrm{CG,d}}(t) & \text{for } \chi = \mathrm{CG}. \end{cases} \tag{55}$$

Because the AG components H_2, N_2, H_2O are mixed before entering the preheater, all components of the AG have one temperature in the interior of the preheater and one in the AG supply line. Analogously, the temperatures at the preheater outlets are denoted by $\vartheta_{\chi}(t)$, while the temperatures at the inlet gas manifold of the SOFC stack are given by $\vartheta_{\chi,\mathrm{in}}(t)$. In good accuracy, it can be assumed during modeling that the AG and CG mass flows can be changed instantaneously. This leads to the definition of *virtual* control signals $v_{\chi,\mathrm{d}}(t)$ in (52). Integrator disturbance models $\dot{\tilde{d}}_{\chi}(t) = 0$ are finally included in the description of the preheaters to account for non-modeled heat losses, thermal storage effects, and imperfect behavior of the underlying temperature control of the AG and CG preheaters.

According to [27], this control-oriented modeling approach leads to a set of input-affine ODEs with the input vector

$$\mathbf{v}_{\mathrm{d}}(t) = \left[v_{\mathrm{H_2,d}}(t) \;\; v_{\mathrm{N_2,d}}(t) \;\; v_{\mathrm{H_2O,d}}(t) \;\; v_{\mathrm{CG,d}}(t) \right]^T \tag{56}$$

of the AG and CG preheaters and the complete state vector

$$\begin{aligned} \mathbf{z}(t) = \Big[& v_{\mathrm{H_2}}(t) \;\; v_{\mathrm{H_2,in}}(t) \;\; \tilde{d}_{\mathrm{H_2}}(t) \;\; v_{\mathrm{N_2}}(t) \;\; v_{\mathrm{N_2,in}}(t) \;\; \tilde{d}_{\mathrm{N_2}}(t) \\ & v_{\mathrm{H_2O}}(t) \;\; v_{\mathrm{H_2O,in}}(t) \;\; \tilde{d}_{\mathrm{H_2O}}(t) \;\; v_{\mathrm{CG}}(t) \;\; v_{\mathrm{CG,in}}(t) \;\; \tilde{d}_{\mathrm{CG}}(t) \\ & \vartheta_{(1,1,1)}(t) \;\; \ldots \;\; \vartheta_{(L,M,N)}(t) \Big]^T \in \mathbb{R}^{\mathcal{N}}, \quad \mathcal{N} = 12 + L \cdot M \cdot N. \end{aligned} \tag{57}$$

If it is assumed that the AG properties are predefined by a subsidiary controller, the ODEs (48) which are extended by the preheater dynamics in (52)–(55) turn into

$$\dot{\mathbf{z}}(t) = \underbrace{\boldsymbol{\phi}_1\left(\mathbf{z}(t), \mathbf{p}\right) + \boldsymbol{\Phi}_{2,\mathrm{AG}}\left(\mathbf{z}(t), \mathbf{p}\right) \cdot \begin{bmatrix} v_{\mathrm{H_2,d}}(t) \\ v_{\mathrm{N_2,d}}(t) \\ v_{\mathrm{H_2O,d}}(t) \end{bmatrix}}_{=: \mathbf{f}_1\left(\mathbf{z}(t), \mathbf{p}, v_{\mathrm{H_2,d}}(t), v_{\mathrm{N_2,d}}(t), v_{\mathrm{H_2O,d}}(t)\right)} + \underbrace{\boldsymbol{\phi}_{2,\mathrm{CG}}\left(\mathbf{z}(t), \mathbf{p}\right) \cdot v_{\mathrm{CG,d}}(t)}_{=: \mathbf{f}_2\left(\mathbf{z}(t), \mathbf{p}, v_{\mathrm{CG,d}}(t)\right)}$$
$$= \mathbf{f}\left(\mathbf{z}(t), \mathbf{p}, \mathbf{v}_{\mathrm{d}}(\mathbf{t})\right). \tag{58}$$

Here, $\boldsymbol{\phi}_1\left(\mathbf{z}(t), \mathbf{p}\right)$ is input-independent, whereas the expression $\mathbf{f}_1\left(\mathbf{z}(t), \mathbf{p}, \ldots\right)$ further contains information about the (desired) AG preheater actuation. The control input $v_{\mathrm{CG,d}}(t)$ is related to the CG enthalpy flow which is coupled with the system dynamics by the vector

$$\boldsymbol{\phi}_{2,\mathrm{CG}}\left(\mathbf{z}(t), \mathbf{p}\right) = \left[\mathbf{0}_{1\times 9}\ \tfrac{1}{T_{\mathrm{CG}}}\ 0\ 0\ \mathbf{0}_{1\times n_x}\right]^T, \quad n_x = L \cdot M \cdot N, \tag{59}$$

where $\mathbf{0}_{i\times j}$ is a zero matrix of dimension $i \times j$ ($n_x = L \cdot M \cdot N$: number of volume elements in the SOFC stack).

If the simplifying assumptions described in [27] are exploited, the equality

$$\frac{\partial \mathbf{f}_1\left(\mathbf{z}(t), \mathbf{p}\right)}{\partial v_{\mathrm{CG,d}}} = \mathbf{0} \tag{60}$$

holds for all operating points. Moreover, choosing $v_{\mathrm{CG,d}}(t)$ as the input justifies the use of $\frac{\mathrm{d}}{\mathrm{d}t}\left[v_{\mathrm{H_2,d}}(t)\ v_{\mathrm{N_2,d}}(t)\ v_{\mathrm{H_2O,d}}(t)\right]^T \approx \mathbf{0}$ during control synthesis. Errors that are caused by this simplification can be taken into consideration by an additive *interval-bounded* disturbance variable in the state-space transformation that is introduced in the following section. This transformation replaces the ODEs (58) by a nonlinear controller canonical form in analogy to (33). Here, the Lie derivatives that are necessary for the definition of the coordinate transformation are computed using techniques for algorithmic differentiation of a corresponding C++ source code of the state equations (58). For details concerning this state-space transformation, see [2, 8, 27].

4 Interval-Based Sliding Mode Control with State and Actuator Constraints for the Thermal Behavior of SOFCs

In this section, the interval-based sliding mode procedures derived in Sect. 2.4 are employed for the robust control of the non-stationary heating phase of the SOFC and for the compensation of disturbances at high-temperature operating points.

4.1 Interval-Based Robust Variable-Structure Control

As shown in Sect. 2.4 and [21, 27], the interval-based variable-structure control approaches make use of system models that are given in a nonlinear controller canonical form.[2] To transform the ODEs (58) into this type of system representation, it is necessary to define the output variable

$$y(t) = h(\mathbf{z}(t)) = \vartheta_{\mathcal{I}^*} \tag{61}$$

as a function of the state vector $\mathbf{z}(t) \in \mathbb{R}^{\mathcal{N}}$. Throughout the remainder of this chapter, the output is defined for each point of time as the maximum segment temperature

$$y(t) = \vartheta_{\mathcal{I}^*}(t) \quad \text{with} \quad \mathcal{I}^* = \arg\max_{\mathcal{I}} \{\vartheta_{\mathcal{I}}(t)\}. \tag{62}$$

The corresponding segment index $\mathcal{I}^*$, the temperature value $y(t)$, and a sufficient number of its time derivatives are estimated in real time by a suitable state observer [24]. The goals of the following control approaches are the accurate tracking of sufficiently smooth desired temperature trajectories during the non-stationary heating phase and the guaranteed prevention of violations of state constraints. For the latter goal it is necessary that the maximum stack temperature does not exceed a predefined upper bound in the high-temperature operating phase despite variations of the electric power demand, variations of the AG properties, and uncertainties in the temperature estimation as well as in the system parameters.

Using this output definition, the system model is transformed into the nonlinear controller canonical form. For this purpose, the Lie derivatives

$$\frac{\mathrm{d}^r y(t)}{\mathrm{d}t^r} = y^{(r)}(t) = L_{\mathbf{f}}^r h(\mathbf{z}(t)) = L_{\mathbf{f}} \left(L_{\mathbf{f}}^{r-1} h(\mathbf{z}(t)) \right), \tag{63}$$

$r = 1, \ldots, \delta$, are computed using techniques for algorithmic differentiation up to the relative degree δ. The relative degree is defined as

$$\frac{\partial L_{\mathbf{f}}^r h(\mathbf{z}(t))}{\partial v_{\mathrm{CG,d}}} \equiv 0 \ \text{ for all } \ r = 0, \ldots, \delta - 1 \quad \text{with} \quad \frac{\partial L_{\mathbf{f}}^{\delta} h(\mathbf{z}(t))}{\partial v_{\mathrm{CG,d}}} \neq 0. \tag{64}$$

Here, $y^{(\delta)}(t)$ is the smallest-order time derivative of $y(t)$ that explicitly depends on the control variable $u(t) = v_{\mathrm{CG,d}}(t)$.

Using the state vector in transformed coordinates

$$\mathbf{x}(t) = \left[h(\mathbf{z}(t)) \ L_{\mathbf{f}} h(\mathbf{z}(t)) \ \ldots \ L_{\mathbf{f}}^{\delta-1} h(\mathbf{z}(t)) \right]^T \in \mathbb{R}^{\delta} \tag{65}$$

[2] Generalized sliding mode-type control procedures, which do not necessarily rely on a transformation into nonlinear controller canonical form, are, for example, described in [29, 30].

with the transformed output variable $x_1(t) := h(\mathbf{z}(t))$, Eq. (58) is rewritten as

$$\begin{aligned}\begin{bmatrix}\dot{\mathbf{x}}(t)\\ \dot{\tilde{\mathbf{x}}}(t)\end{bmatrix} &= \left[\begin{array}{c}\left[L_{\mathbf{f}}h(\mathbf{z})\ \ldots\ L_{\mathbf{f}}^{\delta-1}h(\mathbf{z})\ L_{\mathbf{f}}^{\delta}h(\mathbf{z})\right]^T\\ \hdashline \left[L_{\mathbf{f}}^{\delta+1}h(\mathbf{z})\ \ldots\ L_{\mathbf{f}}^{\mathcal{N}}h(\mathbf{z})\right]^T\end{array}\right]\\ &= \left[\begin{array}{c}\left[x_2(t)\ \ldots\ x_\delta(t)\ \ a(\mathbf{z}(t),\mathbf{p},d(t))\right]^T\\ \hdashline \mathbf{a}^{\diamondsuit}(\mathbf{z}(t),\mathbf{p},d(t))\end{array}\right]\\ &\quad + \left[\begin{array}{c}\left[0\ \ldots\ 0\ \ b(\mathbf{z}(t),\mathbf{p})\cdot v_{\mathrm{CG,d}}(t)\right]^T\\ \hdashline \mathbf{b}^{\diamondsuit}(\mathbf{z}(t),\mathbf{p},d(t),v_{\mathrm{CG,d}}(t),\dot{v}_{\mathrm{CG,d}}(t),\ldots,v_{\mathrm{CG,d}}^{\mathcal{N}-\delta}(t))\end{array}\right]\end{aligned} \tag{66}$$

with the constant but uncertain parameters $\mathbf{p} \in [\mathbf{p}]$ and the additive disturbance $d(t) \in [d] = [\underline{d};\ \overline{d}\,]$. Both of these quantities are assumed to be bounded by closed intervals for the robust sliding mode design.

In (66), the term $a(\mathbf{z}(t),\mathbf{p},d(t))$ is defined by splitting up the Lie derivative $L_{\mathbf{f}}^{\delta}h(\mathbf{z}(t))$ into a purely state-dependent and an input-affine term [27] according to

$$L_{\mathbf{f}}^{\delta}h(\mathbf{z}(t)) = a(\mathbf{z}(t),\mathbf{p},d(t)) + b(\mathbf{z}(t),\mathbf{p})\cdot v_{\mathrm{CG,d}}(t). \tag{67}$$

Here, the disturbance variable $d(t)$ that is included in $a(\mathbf{z}(t),\mathbf{p},d(t))$ is observed in real time. The corresponding estimate $\hat{d}(t)$ is inflated—in analogy to the values $\left[\tilde{\xi}^{(r)}\right](t)$—to the interval $[d] := \hat{d}(t) + \Delta d\cdot[-1;\ 1]$ with $\Delta d > 0$.

Now, all robust sliding mode techniques from Sect. 2.4 can be employed for the SOFC system after setting the output $y(t)$ equal to the state variable $x_1(t) = \vartheta_{\mathcal{I}^*}(t)$. Note that variations of the location at which the maximum stack temperature is expected lead to changes in the actual system output. In such a way, it is possible that non-controllable internal dynamics with the corresponding states $\tilde{\mathbf{x}}(t)$, $\dim\{\tilde{\mathbf{x}}\} > 0$, exist. These state variables are guaranteed to be bounded due to physical conservation properties. This is described in detail in [21, 27]. Since these state variables can be estimated in real time together with the controllable states, they can be treated like time-varying disturbances or parameters during the control design.

During the application of this variable-structure control strategy, the input signal $u(t) = v_{\mathrm{CG,d}}(t)$, determined according to Sect. 2.4 with (37)–(40), (42), or (43), is decomposed into the desired preheater temperature and into the CG mass flow, respectively. Both are optimal in the following sense: Unnecessarily large temporal variations are prevented by soft penalty terms in an online-minimized cost function, while bounds on the admissible minimum and maximum absolute values are treated as hard actuator constraints. A suitable optimality criterion was introduced in [24]. If the CG mass flow is predetermined by an underlying operating strategy of the test rig, the *virtual* input $v_{\mathrm{CG,d}}(t)$ is converted directly into the desired preheater temperature. An overview of the complete control structure can be found in Fig. 6.

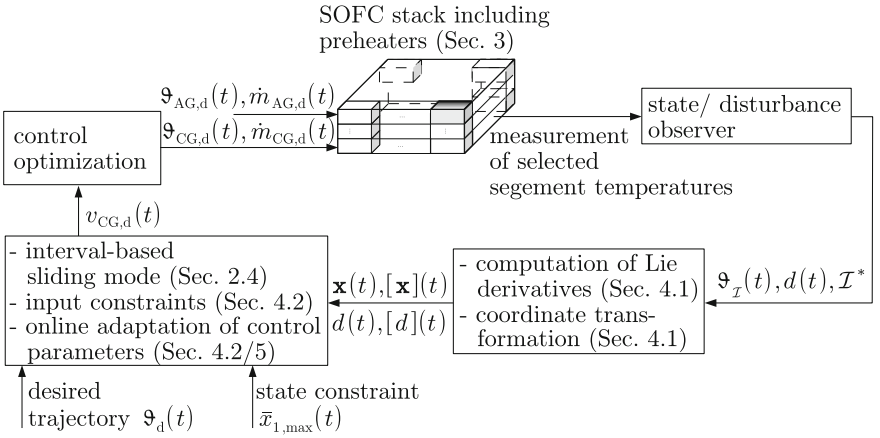

Fig. 6 Structure diagram of the complete variable-structure control law

4.2 Handling of Input and Input Rate Constraints

To make sure that the control strategies derived above can be used on a real test rig, input range as well as rate constraints have to be taken into consideration. On the one hand, this requires—according to the previous subsection—that the control variable $v_{CG,d}(t)$ is decomposed into a product of admissible gas mass flows and desired preheater temperatures. On the other hand, compatibility of the system input with actuator constraints has to be guaranteed by a suitable control parameterization.

In the offline control design of reasonable operating points, a nominal trajectory $x_{1,d}(t)$ is determined for a fixed output segment $\mathcal{I}^*$ with a predefined composition and temperature of the AG. This time-dependent trajectory is selected in such a way that control saturations are not reached for $s = 0$. In the following, this is explained in detail for the case of the first-order sliding mode.

If the nominal state trajectory is compatible with the given constraints, the interval control signal $\left[v_{CG,d}\right](t)$ is split up into a continuous and variable-structure part according to

$$\left[v_{CG,d}\right](t) = \left[v'_{CG,d}\right](t) + \tilde{\eta} \cdot \left[v''_{CG,d}\right](t) \subseteq \left[v_{CG,max}\right]. \tag{68}$$

For a suitable set of asymptotically stable eigenvalues for the dynamics on the sliding surface $s = 0$ and intervals $0 \in \left[\tilde{\xi}^{(r)}\right](t)$ for the operating range, both intervals $[v'_{CG,d}](t)$ and $\left[v_{CG,d}\right](t)$ have to be true subsets $[v'_{CG,d}](t) \subset \left[v_{CG,max}\right]$ and $\left[v_{CG,d}\right](t) \subset \left[v_{CG,max}\right]$ of the maximum possible input range $\left[v_{CG,max}\right]$. Besides an offline adaptation of the variable-structure gain $\tilde{\eta}$ (or the gains $\tilde{\eta}_1$, $\tilde{\eta}_2$ in the second-order case), also a real-time gain scheduling is possible. Both of them lead to adaptations of the parameters $\tilde{\eta}$ and α_r according to the structure diagram in Fig. 7 [22].

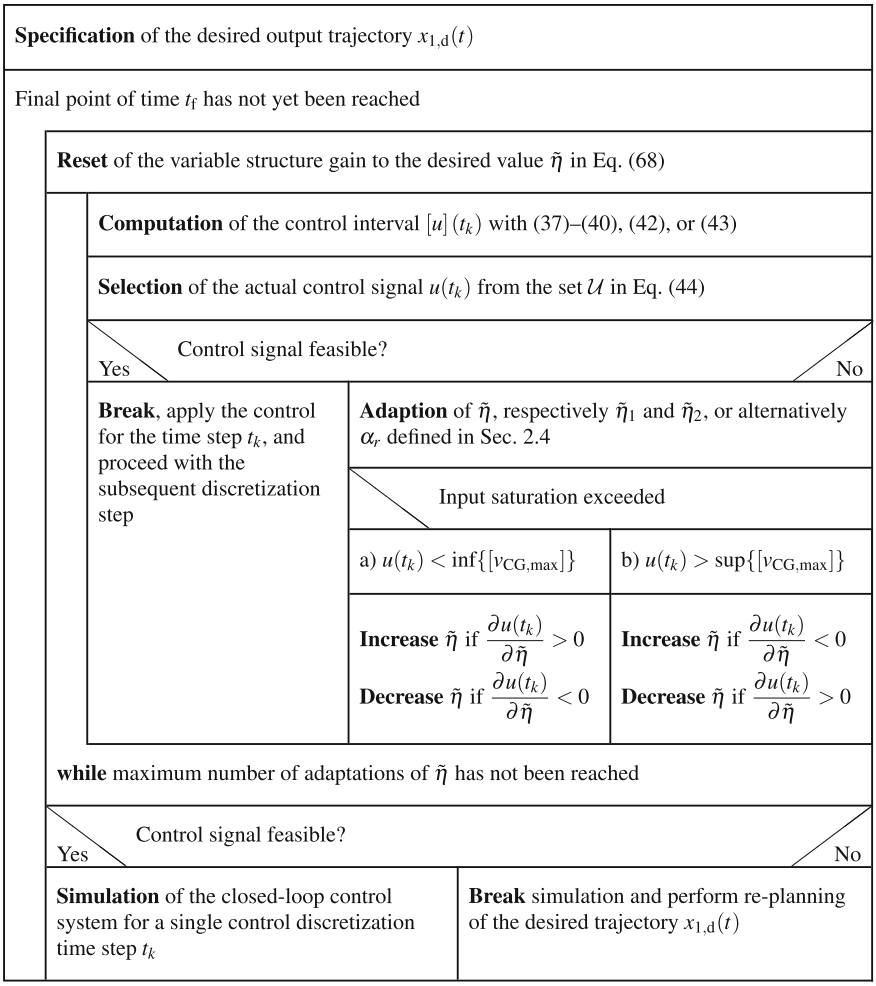

Fig. 7 Trajectory planning and gain scheduling procedure

A simultaneous treatment of hard input range and input rate constraints becomes possible if the first-order lag element

$$T_\mathrm{r} \cdot \dot{v}_{\mathrm{CG,d}}(t) + v_{\mathrm{CG,d}}(t) = \breve{v}_{\mathrm{CG,d}}(t) \quad \text{with the time constant} \quad T_\mathrm{r} > 0 \tag{69}$$

and the new system input $\breve{v}_{\mathrm{CG,d}}(t)$, is appended to the input of the ODE system (58). Equation (69) guarantees that the hard rate constraints

$$\left|\dot{v}_{\mathrm{CG,d}}(t)\right| \leq T_\mathrm{r}^{-1} \cdot \left(\sup\left\{\left[v_{\mathrm{CG,max}}\right]\right\} - \inf\left\{\left[v_{\mathrm{CG,max}}\right]\right\}\right) \tag{70}$$

are automatically satisfied for

$$\inf\left\{\left[v_{\mathrm{CG,max}}\right]\right\} \equiv \inf\left\{\left[\check{v}_{\mathrm{CG,max}}\right]\right\} \quad \text{and} \quad \sup\left\{\left[v_{\mathrm{CG,max}}\right]\right\} \equiv \sup\left\{\left[\check{v}_{\mathrm{CG,max}}\right]\right\}. \tag{71}$$

5 Simulation Results

In this section, different simulation scenarios are compared for the use of interval-based sliding mode controllers for the thermal behavior of SOFCs. In all scenarios, it is assumed that the desired temperature profile for the heating phase of the SOFC stack is given by a sufficiently smooth trajectory $\vartheta_{\mathrm{d}}(t)$ with $t \in [0;\ t^*]$. This trajectory remains constant at $\vartheta_{\mathrm{d}}(t) = \vartheta_{\mathrm{d}}(t^*)$ for $t > t^*$, $t^* = 14{,}000\,\mathrm{s}$.

Throughout the complete heating phase as well as while keeping the stationary high-temperature operating point, the AG mass flows and the AG temperature correspond to those used in [27]. Up to the point $t = t^*$, the AG consists only of preheated nitrogen, while hydrogen is included for the high-temperature phase with $\dot{m}_{\mathrm{H_2}}(t) \neq 0$ and $\frac{\mathrm{d}}{\mathrm{d}t}\dot{m}_{\mathrm{H_2}}(t) \neq 0$ for $t > t^*$. This hydrogen mass flow enables the electrochemical reaction with non-constant electric currents and leads to disturbance heat flows $\dot{Q}^{\mathcal{I}}_{\mathrm{EL}}(t)$ and $\dot{Q}^{\mathcal{I}}_{\mathrm{R}}(t)$ that need to be counteracted by the temperature control approach.

To account for the fact that the SOFC model is only an approximation of the real system dynamics, the additive interval uncertainty $[d]$ is included in the simulation according to

$$[d](t) := [-0.1;\ 0.1] \cdot \left(L^{\delta}_{\mathbf{f}} h(\mathbf{z}(t)) - b(\mathbf{z}(t), \mathbf{p}) \cdot v_{\mathrm{CG,d}}(t)\right). \tag{72}$$

Here, the term in round brackets is evaluated at each point of time $t = t_k$ with a sampling time of 0.5 s. Additionally, it is assumed for all interval-based implementations that the temperature values in the individual finite volume elements $\mathcal{I}$ are not perfectly measurable (or cannot be estimated with absolute accuracy). The corresponding errors are included in the interval $[-15;\ 15]$ K that is added to all temperature values that are involved in the computation of the Lie derivatives in (63)–(66).

Although the two-sided barrier approach included in $u^{\langle \mathrm{I,B} \rangle}(t)$ and $u^{\langle \mathrm{II,B} \rangle}(t)$ can generally be applied to the SOFC system with interval uncertainty, this approach does not allow for a guaranteed handling of hard state constraints. Therefore, only the following options for control parameterizations are considered in this section:

Case (a) $u(t) = u^{\langle \mathrm{I} \rangle}(t)$ with α_r, $\tilde{\eta} = \text{const}$ and $\vartheta_{\mathrm{d}} = 880\,\mathrm{K} = \text{const}$,
Case (b) $u(t) = u^{\langle \mathrm{I,A} \rangle}(t)$ with α_r, $\tilde{\eta} = \text{const}$ and $\vartheta_{\mathrm{d}} = 880\,\mathrm{K} = \text{const}$,
Case (c) $u(t) = u^{\langle \mathrm{I,A} \rangle}(t)$ with α_r, $\tilde{\eta} = \text{const}$ and a time-varying reference signal,
Case (d) $u(t) = u^{\langle \mathrm{I,A} \rangle}(t)$ with online adaptation of the control parameters and a time-varying reference signal.

In the Cases (a)–(c), it is assumed that all coefficients α_r and the variable-structure gain $\tilde{\eta}$ (respectively $\tilde{\eta}_1$ and $\tilde{\eta}_2$) are constant for the complete simulation horizon. The Cases (a) and (b) coincide with scenarios that were already investigated in [21]. In Case (d), an online gain scheduling approach is implemented according to the structure diagram in Fig. 7.

For the Cases (b)–(d), the maximum admissible operating temperature included in the barrier function $V^{\langle \mathrm{A} \rangle}$ is defined as the constant value $\bar{x}_{1,\max} = x_{1,\mathrm{d}}(t) + \Delta x_{1,\max}(t) \equiv 885\,\mathrm{K}$ with

$$V^{\langle \mathrm{A} \rangle} = \rho_{\mathrm{V}} \cdot \sum_{\mathcal{I}} \ln \left(\frac{\sigma_{\mathrm{V}} \cdot \bar{x}_{1,\max}}{\bar{x}_{1,\max} - \vartheta_{\mathcal{I}}(t)} \right). \tag{73}$$

If actuator constraints are violated in the Cases (a)–(c), the system input $u(t) = v_{\mathrm{CG,d}}(t)$ is set equal to the corresponding violated input constraint. Due to the fact that the control parameters α_r, $\tilde{\eta}$ (respectively $\tilde{\eta}_1$ and $\tilde{\eta}_2$) are assumed to be constant in the Cases (a)–(c), the input rate limitation introduced in Eq. (69) has not been accounted for in the computation of the corresponding control signals. However, to make sure that rate constraints are not violated at the actual plant, the control signal is filtered by (69) before applying it at the system input. Ignoring the filter time constant T_{r} during the design stage leads to some amount of chattering due to a model inaccuracy. This inaccuracy is reduced in the scenario (d) by including the filter (69) as an input rate limiter into the controller design. Moreover, the controller parameters are adapted online in the Case (d). Together with the direct inclusion of the input rate limiter (69), this leads to significantly more smooth control inputs and less chattering in the control errors. Furthermore, it yields less conservative choices of the system inputs, which becomes visible by reduced steady-state errors at high-temperature operating points.

Note that all cases in which the barrier functions were active in Figs. 8 and 9 lead to system outputs in which the maximum stack temperatures are compatible with the given state constraint.

In summary, the control implementation that was used in Case (d) of Fig. 9 is advantageous due to the following reasons from a practical point of view: First, the offline design of the desired reference trajectory helps to avoid input saturations for a nominal non-disturbed plant model. Second, the smooth desired reference trajectory for the temperature profile is the major reason why the control in Fig. 9 is generally less aggressive than for a step-like change of the reference signal that was used in Fig. 8. Finally, the online gain adaptation procedure described below for the variable-structure controller reduces chattering to a reasonable level and hence avoids unnecessary actuator wear.

The online parameter adaptation summarized in Fig. 7—which has been applied in Fig. 9—makes use of the following gain scheduling heuristics.

For the first-order sliding mode in the Cases (d), the gain adaptation is performed according to the following:

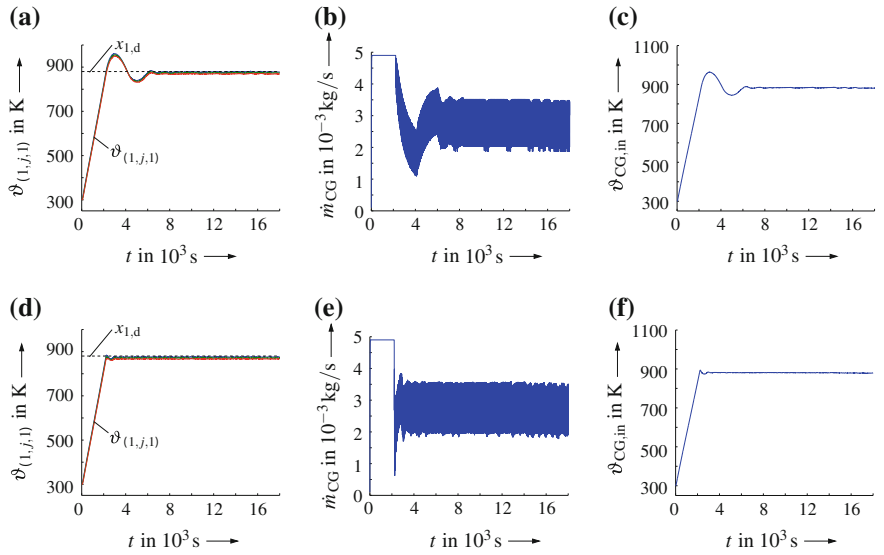

Fig. 8 Comparison of interval-based sliding mode controllers for $L = N = 1$, $M = 3$ without barrier Lyapunov function approach (Case a) and with barrier Lyapunov function (Case b) for a constant desired output $x_{1,d} = 880$ K. **a** Stack temperature (Case a). **b** Mass flow $\dot{m}_{CG}$ (Case a). **c** Temperature $\vartheta_{CG,in}$ (Case a). **d** Stack temperature (Case b). **e** Mass flow $\dot{m}_{CG}$ (Case b). **f** Temperature $\vartheta_{CG,in}$ (Case b)

Step 1. Define a desired eigenvalue λ_r of multiplicity $\delta - 1$ on the sliding surface with corresponding parameters α_r
Step 2. Initialize $\tilde{\eta}$ with the desired value
Step 3. Adapt $\tilde{\eta}$ in a line-search approach (fixed number of $N_\eta = 5$ steps) to ensure compatibility of $u(t) = v_{CG,d}(t)$ with the control constraints

- Stop, if admissible control is found;
- If no admissible control is found within N_η steps, adapt the eigenvalue λ_r and restart with Step 2; Break after at most $N_\lambda = 5$ repetitions.[3]

For the second-order sliding mode, a straightforward extension of the online gain scheduling is given basically by an extension of the previous Step 2.

Step 1. Define a desired eigenvalue λ_r of multiplicity $\delta - 1$ on the sliding surface with corresponding parameters α_r
Step 2a. Initialize both parameters $\tilde{\eta}_1$ and $\tilde{\eta}_2$ with the desired values
Step 2b. Perform one adaptation step of $\tilde{\eta}_2$ according to the sensitivities in Fig. 7
Step 3. Adapt $\tilde{\eta}_1$ in a line-search approach (fixed number of $N_\eta = 5$ steps) to ensure compatibility of $u(t) = v_{CG,d}(t)$ with the control constraints

[3]This limitation is necessary to guarantee real-time applicability of the adaptation procedure.

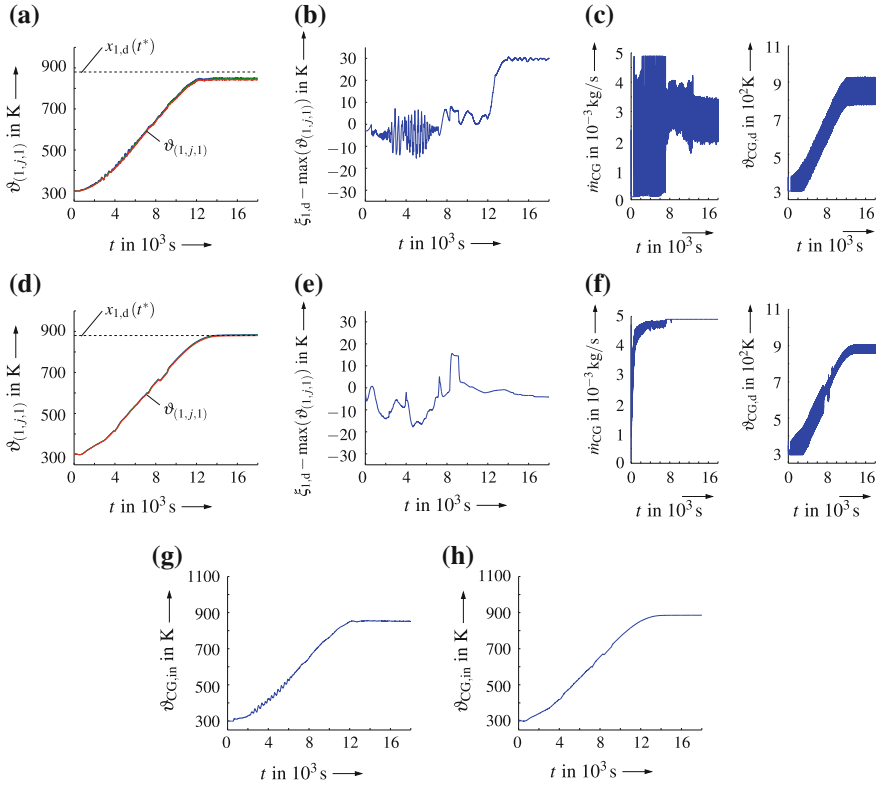

Fig. 9 Comparison of interval-based sliding mode controllers for $L = N = 1$, $M = 3$ with barrier Lyapunov function approach for constant (Case c) and variable controller gains (Case d) for a time-varying desired output $x_{1,\mathrm{d}}(t) \neq \text{const}$. **a** Stack temperature (Case c). **b** Tracking error (Case c). **c** CG control inputs (Case c). **d** Stack temperature (Case d). **e** Tracking error (Case d). **f** CG control inputs (Case d). **g** CG stack inlet temperature (Case c). **h** CG stack inlet temperature (Case d)

- Stop, if admissible control is found;
- Repeat the Steps 2b and 3 for a maximum of $M_\eta = 5$ times, where the restart of Step 3 is performed with the originally desired parameter $\tilde{\eta}_1$;
- If no admissible control is found within $M_\eta \cdot N_\eta$ steps, adapt the eigenvalue λ_r and restart with Step 2a; Break after at most $N_\lambda = 5$ repetitions.

Note that both adaptation procedures ensure stability for $\Re\{\lambda_r\} < 0$ and $\tilde{\eta} > 0$ as well as $\tilde{\eta}_1 > 0$ and $\tilde{\eta}_2 > 0$. However, simulation case studies have shown that the control performance may become worse if sign (s) changes its value during the parameter adaptation. This can be prevented by adding an additional term $-\nu(t)$ with

$$\nu(t) \begin{cases} < 0 & \text{for} \quad \inf\{-[\vartheta_{\mathcal{I}^*}](t) + x_{1,\mathrm{d}}\}(t) < 0 \\ > 0 & \text{for} \quad \sup\{-[\vartheta_{\mathcal{I}^*}](t) + x_{1,\mathrm{d}}\}(t) > 0 \\ = 0 & \text{else} \end{cases} \tag{74}$$

onto the numerators of (37) and (40), respectively. Note that the intervals on the right-hand side of (74) reflect the measurement or state reconstruction tolerances of the stack module temperatures. In cases in which the adaptation of the parameters according to Fig. 7 leads to a change of sign (s), the absolute value of $\nu(t)$ needs to be chosen in the following manner: If the Steps 1–3 yield no admissible solution with the same sign of s as the initialization, the term $-\nu(t)$ is selected in such a way that the control is set exactly to the respective bound of the input $u(t) = v_{\mathrm{CG,d}}(t)$ that was originally violated. According to the simulations in Fig. 9, this measure preserves the desired stability properties and still prevents overshooting the maximum admissible stack temperature, however, without a formal proof.

6 Conclusions and Outlook

In this chapter, various generalizations of sliding mode controllers were presented toward interval-based implementations. These implementations focus on a guaranteed stabilization of sets of ODEs describing the dynamics of closed-loop control systems with uncertain parameters and uncertain state variables. Both of these uncertain quantities are assumed to be represented by closed intervals. Despite the aim of a guaranteed stabilization of the control error dynamics in such uncertain settings, further generalizations were discussed for a reliable treatment of state and actuator constraints. Especially, the overshoot prevention of given upper state boundaries and the treatment of input range and input rate constraints were visualized for the control of the thermal behavior of a high-temperature fuel cell system.

It has been shown that the presented approaches lead to a guaranteed compatibility of the closed-loop dynamics with the before-mentioned constraints as well as with robustness and stability requirements. Moreover, an online parameter adaptation approach was validated in simulations which allows for a reduction of chattering if constant control parameters may cause the violation of input range constraints. Classically, such violations are purely avoided by corresponding saturation elements.

Future work will deal with further generalizations of the controller, e.g., with parameterizations of the system input by time-dependent polynomials. In such a way, it is desired to further smoothen the inputs when treating the polynomial coefficients as virtual inputs that are alternatively computed by sliding mode or predictive control techniques. Moreover, generalizations of the presented quasi-continuous variable-structure control approaches toward a discrete-time implementation may be investigated in the future.

References

1. Bartolini G, Pisano A, Punta E, Usai E (2003) A survey of applications of second-order sliding mode control to mechanical systems. Int J Control 76(9–10):875–892
2. Bendsten C, Stauning O (2007) FADBAD++, Version 2.1, http://www.fadbad.com
3. Bove R, Ubertini S (eds) (2008) Modeling solid oxide fuel cells. Springer, Berlin
4. Eker Í (2010) Second-order sliding mode control with experimental application. ISA Trans 49(3):394–405
5. Fliess M, Lévine J, Martin P, Rouchon P (1995) Flatness and defect of nonlinear systems: introductory theory and examples. Int J Control 61:1327–1361
6. Fortmann TE, Hitz KL (1977) An introduction to linear control systems. Marcel Dekker Inc, New York
7. Fridman L, Levant A (2002) Higher order sliding modes. In: Barbot JP, Perruguetti W (eds) Sliding mode control in engineering. Marcel Dekker, New York, pp 53–101
8. Griewank A, Walther A (2008) Evaluating derivatives: principles and techniques of algorithmic differentiation. SIAM, Philadelphia
9. Han SI, Cheong JY, Lee JM (2013) Barrier Lyapunov function-based sliding mode control for guaranteed tracking performance of robot manipulator. Mathematical problems in engineering. Hindawi Publishing Corporation, Article ID 978241, 9 p. doi:10.1155/2013/978241
10. Huang B, Qi Y, Murshed AKMM (2013) Dynamic modeling and predictive control in solid oxide fuel cells: first principle and data-based approaches. Wiley, Chichester
11. Jaulin L, Kieffer M, Didrit O, Walter É (2001) Applied interval analysis. Springer, London
12. Khalil HK (2002) Nonlinear systems, 3rd edn. Prentice-Hall, Upper Saddle River
13. Krämer W (2012) XSC languages (C-XSC, PASCAL-XSC) — scientific computing with validation, arithmetic requirements, hardware solution and language support. www.math.uni-wuppertal.de/~xsc/, C-XSC 2.5.3
14. Krasnochtanova I, Rauh A, Kletting M, Aschemann H, Hofer EP, Schoop KM (2010) Interval methods as a simulation tool for the dynamics of biological wastewater treatment processes with parameter uncertainties. Appl Math Model 34(3):744–762
15. Marquez H (2003) Nonlinear control systems. Wiley, New Jersey
16. Moore R (1966) Interval arithmetic. Prentice-Hall, Englewood Cliffs
17. Niu B, Zhao J (2013) Barrier Lyapunov functions for the output tracking control of constrained nonlinear switched systems. Syst Control Lett 62(10):963–971
18. Pukrushpan J, Stefanopoulou A, Peng H (2005) Control of fuel cell power systems: principles, modeling, analysis and feedback design, 2nd edn. Springer, Berlin
19. Rauh A, Aschemann H (2012) Interval-based sliding mode control and state estimation for uncertain systems. In: Proceedings of IEEE international conference on methods and models in automation and robotics MMAR 2012. Miedzyzdroje, Poland
20. Rauh A, Senkel L, Aschemann H (2014) Variable structure approaches for temperature control of solid oxide fuel cell stacks. In: Proceedings of 2nd international conference on vulnerability and risk analysis and management ICVRAM 2014. Liverpool, UK
21. Rauh A, Senkel L, Aschemann H (2015) Interval-based sliding mode control design for solid oxide fuel cells with state and actuator constraints. IEEE Trans Ind Electron 62(8):5208–5217
22. Rauh A, Senkel L, Aschemann H (2015) Reliable sliding mode approaches for the temperature control of solid oxide fuel cells with input and input rate constraints. In: Proceedings of 1st IFAC conference on modelling, identification and control of nonlinear systems, MICNON 2015. St. Petersburg, Russia
23. Rauh A, Senkel L, Auer E, Aschemann H (2014) Interval methods for the implementation of real-time capable robust controllers for solid oxide fuel cell systems. Math Comput Sci 8(3–4):525–542
24. Rauh A, Senkel L, Dötschel T, Auer E, Aschemann H (2014) Numerical verification and experimental validation of sliding mode control design for uncertain thermal SOFC models. Reliab Comput 19(4):330–350

25. Rauh A, Senkel L, Kersten J, Aschemann H (2013) Verified stability analysis for interval-based sliding mode and predictive control procedures with applications to high-temperature fuel cell systems. In: Proceedings of 9th IFAC symposium on nonlinear control systems. Toulouse, France
26. Rauh A, Senkel L, Kersten J, Aschemann H (2014) Interval methods for sensitivity-based model-predictive control of solid oxide fuel cell systems. Reliab Comput 19(4):361–384
27. Rauh A, Senkel L, Kersten J, Aschemann H (2014) Reliable control of high-temperature fuel cell systems using interval-based sliding mode techniques. IMA J Math Control Inf (available online). doi:10.1093/imamci/dnu051
28. Senkel L, Rauh A, Aschemann H (2013) Experimental validation of a sensitivity-based observer for solid oxide fuel cell systems. In: Proceedings of IEEE international conference on methods and models in automation and robotics MMAR 2013. Miedzyzdroje, Poland
29. Senkel L, Rauh A, Aschemann H (2014) Sliding mode techniques for robust trajectory tracking as well as state and parameter estimation. Math Comput Sci 8(3–4):543–561
30. Senkel L, Rauh A, Aschemann H (2016) Experimental and numerical validation of a reliable sliding mode control strategy considering uncertainty with interval arithmetic. In: Rauh A, Senkel L (eds) Variable-structure approaches for analysis, simulation, robust control and estimation of uncertain dynamic systems, mathematical engineering. Springer, Berlin, pp 87–122. doi:10.1007/978-3-319-31539_4
31. Shtessel Y, Edwards C, Fridman L, Levant A (2014) Sliding mode control and observation. Springer, New York
32. Slotine JJE, Li W (1991) Applied nonlinear control. Prentice Hall, Eaglewood Cliffs
33. Stiller C (2006) Design, operation and control modelling of SOFC/GT hybrid systems. Ph.D. thesis, University of Trondheim
34. Stiller C, Thorud B, Bolland O, Kandepu R, Imsland L (2006) Control strategy for a solid oxide fuel cell and gas turbine hybrid system. J Power Sources 158:303–315
35. Tee KP, Ge SS, Tay EH (2009) Barrier Lyapunov functions for the control of output-constrained nonlinear systems. Automatica 45(4):918–927
36. Utkin V (1992) Sliding modes in control and optimization. Springer, Berlin
37. Utkin V (1993) Sliding mode control design principles and applications to electric drives. IEEE Trans Ind Electron 40(1):23–36